



January 2018

The Application Of Nanoindentation Technology With Simulation On The Micromechanical Properties Of Bakken Formation

Hao Fu

Follow this and additional works at: <https://commons.und.edu/theses>

Recommended Citation

Fu, Hao, "The Application Of Nanoindentation Technology With Simulation On The Micromechanical Properties Of Bakken Formation" (2018). *Theses and Dissertations*. 2214.
<https://commons.und.edu/theses/2214>

This Thesis is brought to you for free and open access by the Theses, Dissertations, and Senior Projects at UND Scholarly Commons. It has been accepted for inclusion in Theses and Dissertations by an authorized administrator of UND Scholarly Commons. For more information, please contact zeinebyousif@library.und.edu.

THE APPLICATION OF NANOINDENTATION TECHNOLOGY WITH
SIMULATION ON THE MICROMECHANICAL PROPERTIES OF
BAKKEN FORMATION

by

Hao Fu
Bachelor of Science, Civil Aviation University of China, 2016

A Thesis

Submitted to the Graduate Faculty

of the

University of North Dakota

In partial fulfillment of the requirements

for the degree of
Master of Science

Grand Forks, North Dakota

May
2018

This thesis, submitted by Hao Fu in partial fulfillment of the requirements for the Degree of Master of Science from the University of North Dakota, has been read by the Faculty Advisory Committee under whom the work has been done and is hereby approved.



Hui Pu, Ph.D.,-Chairperson




Kegang Ling, Ph.D.,-Committee Member



Vamegh Rasouli, Ph.D.,-Committee Member

This thesis is being submitted by the appointed advisory committee as having met all of the requirements of the School of Graduate Studies at the University of North Dakota and is hereby approved.



Dr. Grant McGimpsey
Dean of the School of Graduate Studies
4/25/18

Date

PERMISSION

Title The Application of Nanoindentation Technology with Simulation on
the Micromechanical Properties of Bakken Formation

Department Petroleum Engineering

Degree Master of Science

In presenting this thesis in partial fulfillment of the requirements for a graduate degree from the University of North Dakota, I agree that the library of this University shall make it freely available for inspection. I further agree that permission for extensive copying for scholarly purposes may be granted by the professor who supervised my thesis work or, in his absence, by the Chairperson of the department or the dean of the School of Graduate Studies. It is understood that any copying or publication or other use of this thesis or part thereof for financial gain shall not be allowed without my written permission. It is also understood that due recognition shall be given to me and to the University of North Dakota in any scholarly use which may be made of any material in my thesis.

Hao Fu

May 3, 2018

TABLE OF CONTENTS

LIST OF FIGURES	vi
LIST OF TABLES	vii
ACKNOWLEDGEMENTS	viii
ABSTRACT	x
CHAPTER	
I. INTRODUCTION	1
Background	1
Research Significance	3
Methods	4
Anticipated Results	5
II. BACKGROUND AND LITERATURE REVIEW	6
The Purpose of Nanoindentation	6
Geologic Structure of Bakken Formation	7
Mineral Compositions of Formation Rock	8
The Approaches for Studying on Rock Properties	9
III. THE APPLICATION OF NANO-TECHNOLOGY ON SHALE	10
Sample Preparation	10
SEM on the Sample Surface	12
XRD for Analyzing Chemical Element	15
Nanoindentation Test	19

IV.	SIMULATION OF ROCK PROPERTIES	30
	Introduction of Finite Element Analysis	30
	Application of ANSYS on Shale	31
	Building of Geometry Model.....	33
	Solution.....	35
	Postprocessing.....	36
	Results of Simulation and Analysis.....	39
V.	CONCLUSIONS.....	44
	APPENDICES	46
	APPENDIX A	47
	APPENDIX B.....	48
	APPENDIX C.....	49
	NOMENCLATURE.....	57
	REFERENCES.....	58

LIST OF FIGURES

Figure	Page
1. Map of Bakken Formation.....	1
2. Generalized stratigraphic chart and associated total petroleum system for the Williston Basin.....	3
3. The shape and geology structure of Bakken shale.....	8
4. (a) Section of Middle Bakken Core for sample #1 and (b) Core fragments prepared in epoxy of sample #1 for nanoindentation tests.....	11
5. (a) Section of cores from Bakken for samples #2, #3, #4, #5 and (b) Sample chips in epoxy for nanoindentation tests for samples #2, #3, #4, #5.....	12
6. Hitachi S-3400NH scanning electron microscope.....	13
7. (a) SEM image of the chip in sample#1 whose surface is parallel to the bedding of Middle Bakken Formation and (b) SEM image of the chip in sample#1 whose surface is perpendicular to the bedding of Middle Bakken Formation.....	14
8. SEM image of sample #2 of Middle Bakken	15
9. Rigaku SmartLab X-ray diffraction system.....	16
10. Profile of mineral percentage in sample #1	17
11. Profile of mineral percentage in sample #2.....	19
12. Hysitron TI-700 ubi Nano-mechanical indenter.....	20
13. The curve of loading-unloading in the process of indentation.....	21
14. An array of 4×4 indentations on the rock sample.....	22
15. Young’s modulus vs. hardness for all indentations on sample #1 (Indentations perpendicular to the bedding of Middle Bakken).....	23
16. Young’s modulus vs. hardness for all indentations on sample #1 (Indentations parallel to the bedding of Middle Bakken)	23
17. Average Young’s modulus vs. number of indentations on sample #1 (Indentations perpendicular to the bedding of Middle Bakken).....	24

18. Average Young’s modulus vs. number of indentations on sample #1 (Indentations parallel to the bedding of Middle Bakken).....	25
19. Average hardness vs. number of indentations on sample #1 (Indentations perpendicular to the bedding of Middle Bakken).....	26
20. Average hardness vs. number of indentations on sample #1 (Indentations parallel to the bedding of Middle Bakken).....	26
21. Average Young’s modulus vs. number of indentations on sample #2 of Middle Bakken.....	27
22. Average hardness vs. number of indentations on sample #2 of Middle Bakken.....	28
23. Young’s modulus vs. hardness for all indentations on sample #2 of Middle Bakken.....	28
24. Schematic illustration of nanoindentation process	32
25. (a) Isometric view of the finite element mesh used for the nanoindentation simulation and (b) Detailed meshing near contact area.....	35
26. (a) Image of deformed shape after loading in simulation and (b) Detailed deformation near contact area.....	38
27. Von Mises Stress distribution of rock sample #1.....	39
28. Experimental curve of nanoindentation process for sample #1.....	40
29. The relationship of displacement and force in simulation for sample #1.....	41
30. Experimental curve of nanoindentation process for sample #2.....	42
31. The relationship of displacement and force in simulation for sample #2.....	43

LIST OF TABLES

Table	Page
1. Basic information of sample sources.....	10
2. The Weight percentage of each mineral in sample #1.....	17
3. The Weight percentage of each mineral in sample #2.....	18
4. Material properties used in numerical simulation.....	32

ACKNOWLEDGEMENTS

I would like to thank my committee members Dr. Hui Pu, Dr. Kegang Ling and Dr. Vamegh Rasouli. Especially thanks to Dr. Pu and Dr. Ling's patient and serious instruction. Under their advice and encourage, I used to study for my master degree with an enjoyable mood during last two years. Also, I want to thank all the faculty at petroleum department in college of engineering & mines for your impartment of knowledge without any reservation.

I would like to thank Dr. Xiaodong Hou and Mr. Jun Ge for their help when I did experiments for research. Their intelligence and critical thinking gave me much enlightenment in studying process.

Here, I also would like to thank all my classmates who provided me suggestions for my research.

Finally, I would like to thank all the love and support from my great parents.

ABSTRACT

The application of hydraulic fracturing technology has caused a boom in Bakken oil production since 2000. The geomechanics tests need to be used in optimization of hydraulic design and mechanical properties are important factors that control or influence fracture geometry. Conventionally, in order to know Young's modulus, the industry either uses cores to carry out dynamic and static tests on plugs or sonic logs. These methods are more expensive comparing with nanoindentation.

In this study, nanoindentation tests were performed on core samples from Middle and Lower Bakken Formation. This work is especially useful for the optimization of drilling activities, as well as hydraulic fracturing operations in Bakken fields.

Finite element method has been extensively used to characterize mechanical properties of rock samples from Bakken formation by simulating nanoindentation procedures. The information from strain can help us to obtain the basic properties of rock samples.

CHAPTER I

INTRODUCTION

The Bakken formation has become in last few years as one of the most crucial energy sources in the United States. The region of the Bakken formation includes North Dakota, Montana, Saskatchewan and Manitoba, as shown in Figure 1. The application of hydraulic fracturing and horizontal drilling has been widely used in Bakken formation since 2000 and in the year of 2014, and due to this North Dakota became the second-largest oil production state in the United States.

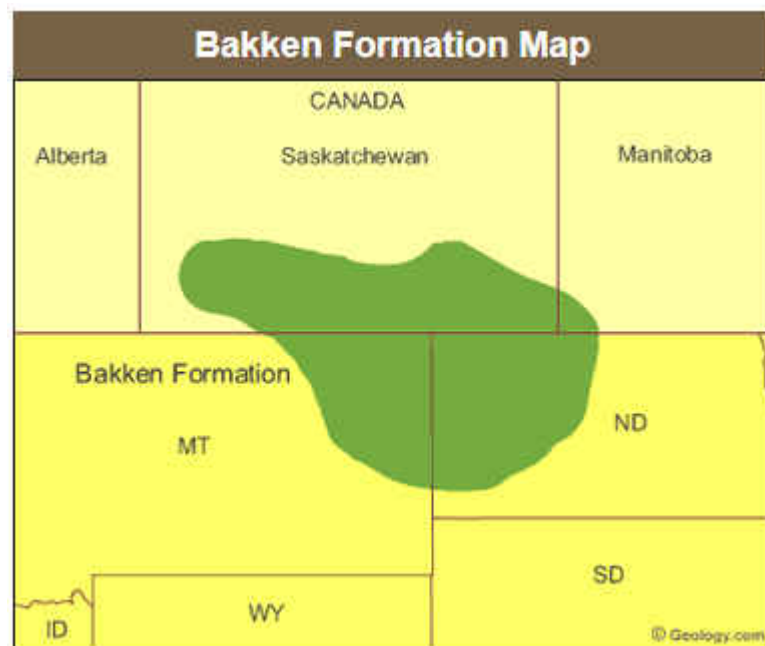


Figure 1. Map of Bakken Formation (source: www.geology.com)

Background

Bakken formation is overlaid by the Mississippian age Lodgepole Limestone

formation and Three Forks formation is overlaid by the Devonian age as shown in Figure 2. The lithology of the Middle Bakken varies somewhat unpredictably from a light-to-medium gray, very-dolomitic fine-grained siltstone to a very silty, fine-crystalline dolomite (Wang and Zeng, 2011). Dark carbonaceous mottles and partings are commonly present. The Middle member is often faintly laminated, and occasionally contains fine-scale cross-bedding (Wang and Zeng, 2011). The hydrocarbon source rocks are the Upper and Lower members, which are organic-rich, with total organic carbon (TOC) content ranging from 12 to 36wt%, average 25 to 28wt% over large portions of the basin (Tran et al., 2011). The Middle Bakken member, which is the primary oil target, is an organic-lean interval. The average depth of the Middle Bakken is about 10,000 ft. The porosity of the Middle Bakken is about 6% and the permeability averages 0.001–0.01mD or less. Water saturation varies between 25% and 50% in the Middle Bakken (Cherian et al., 2012). The average oil gravity is about 42 °API. Gas oil ratio (GOR) ranges from 507 to 1712 SCF/STB, and the bubble point pressure varies from 1,617 to 3,403 psi (Nojabaei et al., 2013). The Bakken formation is variably overpressured with pressure gradients up to 0.73 psi/ft in the central part of the basin (Meissner, 1978).

Over the past two decades, there has been an increased interest in how nanoscale and microscale structure impact mechanical properties (Bhowmik et al., 2007; Ghosh et al., 2007; Katti et al., 2013). The nanoindentation test can be conducted on small size (e.g. millimeter) rock samples, for instance, drill cuttings can be experimental subject for nanoindentation testing. Nanoindentation testing on drill cuttings, small pieces taken from core plugs, and sidewall cores can be used to obtain a reliable measurement of

Young's modulus which is an important parameter used in hydraulic fracturing design (Shukla et al., 2013). The primary objective of this study is to apply the nanoindentation measurement technique on shales for the measurement of the mechanical properties of rock materials, with a goal to achieve a more accurate characterization of material properties. Toward the end, this study integrates the laboratory nanoindentation test with scanning electron microscope (SEM) and X-ray diffraction (XRD) analysis.

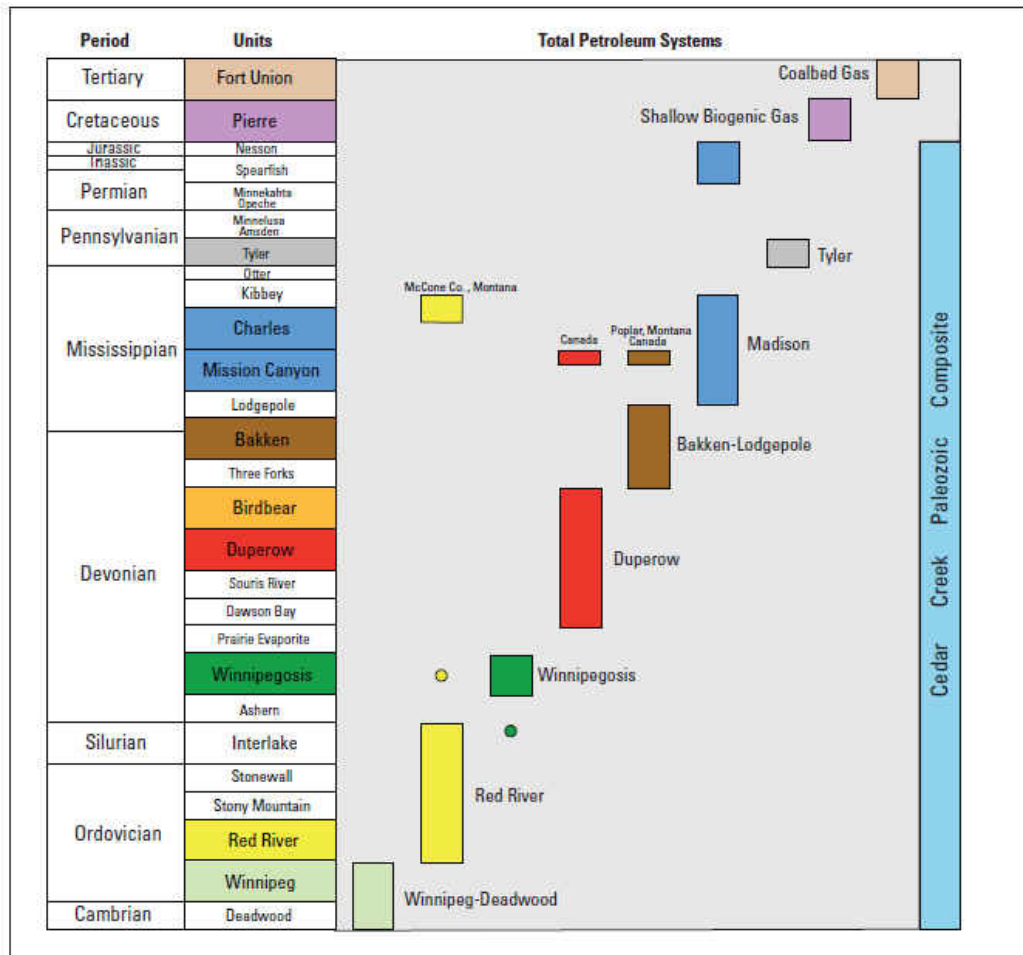


Figure 2. Generalized stratigraphic chart and associated total petroleum system for the Williston Basin (Anna et al., 2013)

Research Significance

The significance of the study is to find the mechanical properties of rock

samples from Bakken Formation. These rock properties such as Young's modulus and hardness are very important for drilling. Bakken formation is one of the biggest unconventional oilfields in the United States. With regards to unconventional resources, hydraulic fracturing method is widely used in extracting oil and natural gas from shale reservoirs. The geomechanics tests need to be used in optimization of hydraulic fracturing design and mechanical properties are important factors that control or influence fracture geometry. Conventionally, in order to know Young's modulus, the industry either uses cores to carry out dynamic and static tests on plugs or sonic logs. These methods are more expensive comparing with nanoindentation.

Methods

The Nanoindentation is a technique used to measure the mechanical properties of rock samples. The technique was performed on core samples from Middle and Lower Bakken Formation using Hysitron Nano Mechanical Test Instrument. Bedding directions were marked, and nanoindentation tests measured properties of samples which are parallel and perpendicular to the bedding of Bakken formation. The measurement results were compared with each other and rock samples from different depths of wells were used to discover the relationships among rock properties, well depth and formation type. In addition, statistics methods have been applied to obtain macro-mechanical properties through micro properties for rock samples.

Finite element method (FEM) has been extensively used to characterize mechanical properties of rock samples by simulating nanoindentation procedures. FEM can be used to study the complex stress and strain area under nanoindenter tip which is not easy to be known by experiment. The information from strain can help to obtain the

basic properties of rock samples, such as Young's modulus, hardness, etc.

From the estimation of experimental results, different samples have different properties due to the heterogeneity of Bakken. FEM simulation resolves the disadvantages of the experiment such as stress distribution and displacement curve at contact area, temperature effects and complex geometry, etc. So using nanoindentation technology combining with FEM simulation can help to investigate the rock properties of Bakken precisely.

Anticipated Results

Micromechanical properties including hardness, Young's modulus, and penetration depth are very important for Middle and Lower Bakken Formations. In order to figure out the mechanical properties of Bakken Formation, the methods of nanoindentation, XRD and SEM were used for the samples from Middle and Lower Bakkens. Comparing with the conventional method, Young's modulus and hardness in the micro scale can be easily obtained via nanoindentation test. The scanning electron microscope with energy-dispersive spectroscopy was used to observe the mineral distribution on the surface of the rock. The function of X-ray diffraction was utilized to analyze mineral compositions of the rock. In nanoindentation tests, for the samples in the different depths of the same well, the values of Young's modulus varied according to the difference of depths. Core samples can be measured by using nanoindentation test, which could provide means for studying the micromechanical properties effected by mineralogy and organic matter.

CHAPTER II

BACKGROUND OF LITERATURE REVIEW

The Purpose of Nanoindentation

So far, nanoindentation technology has been widely applied to the material area. However, comparing with the high oil production of Bakken Formation, the research on Bakken Formation still needs to be improved. Through the research from other people, it is obvious that using simulation software ANSYS Mechanical APDL 18.1 is suitable to compare with the result of experiments in order to measure mechanical properties accurately.

Nanoindentation can be used to measure the mechanical properties of samples with very small size. In this study, nanoindentation tests were performed on five core samples from the Bakken Formation. At first, for one of these five samples, bedding directions of the Middle Bakken were marked, and nanoindentation tests were used to measure the properties of chips in the sample whose surface are parallel and perpendicular to the bedding, respectively. Then the measurement results were summarized and compared for the perpendicular indentation and parallel indentation on chips. Next, for another four samples obtained from different depths of various wells in Bakken Formation, the method of nanoindentation was used to explore the relationships among Young's modulus, hardness and contact depth during the experiments.

In addition, mineral composition analysis and scanning electron microscope (SEM) with energy-dispersive X-ray spectroscopy (EDS) analysis were performed to

characterize the microfabric of the samples, and the morphology, size and distribution of the minerals for Bakken samples.

Geologic Structure of Bakken Formation

The Williston Basin is one of the most structurally simple basins in the U.S. The basin takes the shape of a saucer or bowl being the deepest near Williston in North Dakota, as shown in Figure 3.

The Bakken Formation formed during the late Devonian and early Mississippian age, which is included in the Kaskaskia Sequence (Hester et al., 1985). The area of Bakken Formation covers the states of Montana, North Dakota in the U.S. and the provinces of Manitoba and Saskatchewan in Canada. According to the depth of Bakken Formation, three layers mainly constituted the rock formation which are upper shale layer, middle silty dolomite and lower shale layer. The Upper and Lower Bakken Members have apparently identical lithologies throughout most of their areal extent, and consist of hard brittle waxy-looking black shale (Wang et al., 2011). The Bakken Formation is sealed by Three Forks Sanish Formation, which composed of dolomite and mudstone primarily. The estimate of original oil in place (OOIP) for the Bakken Formation ranges from 200 to more than 400 billion barrels (Price, 2000). This unconventional reserve in the Bakken Formation becomes increasingly important when the growth rate of demand outpaces one of new reserves on oil and gas (Jun, 2015).

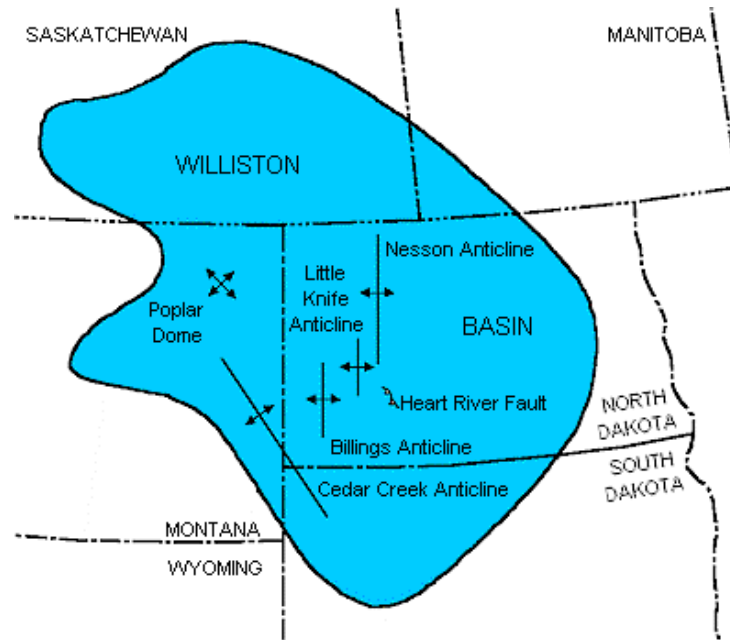


Figure 3. The shape and geology structure of Bakken shale (source: bakkenshale.com)

Mineral Compositions of Formation Rock

Bakken formation has different types of rock and minerals. Rock compositional data for the investigated Bakken Shale samples are subdivided into three groups: (1) clay minerals (illite, chlorite, kaolinite, mica, etc.); (2) carbonate minerals (calcite and dolomite); and (3) quartz and feldspar. (Ming, 2016). Illite is composed of elements such as Si, Al, K and minor Mg, Ca, Fe. Illite is similar in chemical composition to phlogopite, but phlogopite has Ti and more Mg. Chlorite is made up of Si, Al, Mg and Fe. Kaolinite ($Al_2Si_2O_5(OH)_4$) is a clay mineral which is mainly composed of Si and Al. Calcite ($CaCO_3$) is a carbonate mineral which is colorless or white usually. The formula of dolomite is $CaMg(CO_3)_2$. Dolomite often contains silicon, iron, aluminum, titanium and other impurities. Quartz (SiO_2) often contains a small number of impurity components so it becomes translucent or opaque crystals from colorless and transparent crystals. Also, quartz has hard texture. Feldspars may comprise any of the

aluminosilicates of potassium, sodium and calcium (Ming, 2016). Pyrite (FeS_2) is a brassy and brittle mineral which is easily broken by striking.

The Approaches for Studying on Rock Properties

The conventional method to measure the rock properties is core analysis. Laboratory measurement procedures and conditions affect core analysis data quality and accuracy (Ma et al., 2002).

Usually, standard core plugs were cut for the initial, routine core analysis program consisting of unstressed porosity and air permeability measurements. A subset of core plug samples was selected for additional specialized measurements utilizing internal laboratory capabilities. The specialized core measurements included porosity and brine permeability at in situ and variable stress, and acoustic velocity. Data such as these can be of general use, but are not considered sufficiently accurate for quantitative rock properties model calibration. Also, the method of core analysis is expensive and tedious. Hence, cheaper methods to measure rock properties are preferred, such as nanoindentation technology. Nanoindentation experiment is convenient and cheap for determining rock micromechanical properties. Nano-scale response from different grains can be obtained with high accuracy and precision. Therefore, nanoindentation tests are more and more widely applied to measure rock properties in the industry.

CHAPTER III

THE APPLICATION OF NANO-TECHNOLOGY ON SHALE

Sample Preparation

The five core samples of Bakken Formation were collected from the North Dakota Geological Survey's Wilson M. Laird Core and Sample Library (Table 1). Figure 4(a) shows the Middle Bakken core slab from a well from which sample #1 shown in Figure 4(b) were obtained. In Figure 4(b) one polished surface of a chip is parallel the bedding of Middle Bakken, the other chip's polished surface is vertical to the bedding of Middle Bakken Formation. The samples in Figure 5(b) were chosen from the core slab in Figure 5(a). Small chips were selected from the representative cores at certain depths, then samples were cast in the form of a disc using epoxy in the mold. Subsequently, they were polished prior to nanoindentation tests. The preparation of smooth sample surface is crucial for nanoindentation experiments. The samples were polished using silicon carbide abrasive papers from grit size of 80 to 1,200, followed by 3 μ m and 1 μ m diamond paste. After that, they were dried and put under a suitable condition for storage. The core sample descriptions can be found in Appendix A.

Table 1. Basic information of sample sources

Sample Number	Well Name	Depth (ft)	Formation
#1	LINSETH 13-12HW	11135.40	Middle Bakken
#2	Chruszch 43-29F	10888.35	Middle Bakken

Table 1. cont.

Sample Number	Well Name	Depth (ft)	Formation
#3	Chruszch 43-29F	10932.95	Lower Bakken
#4	Pumpkin 148-93-14C-13H TF	10249.00	Lower Bakken
#5	Pumpkin 148-93-14C-13H TF	10309.00	Lower Bakken



(a)



(b)

Figure 4. (a) Section of Middle Bakken Core for sample #1 and (b) Core fragments prepared in epoxy of sample #1 for nanoindentation tests

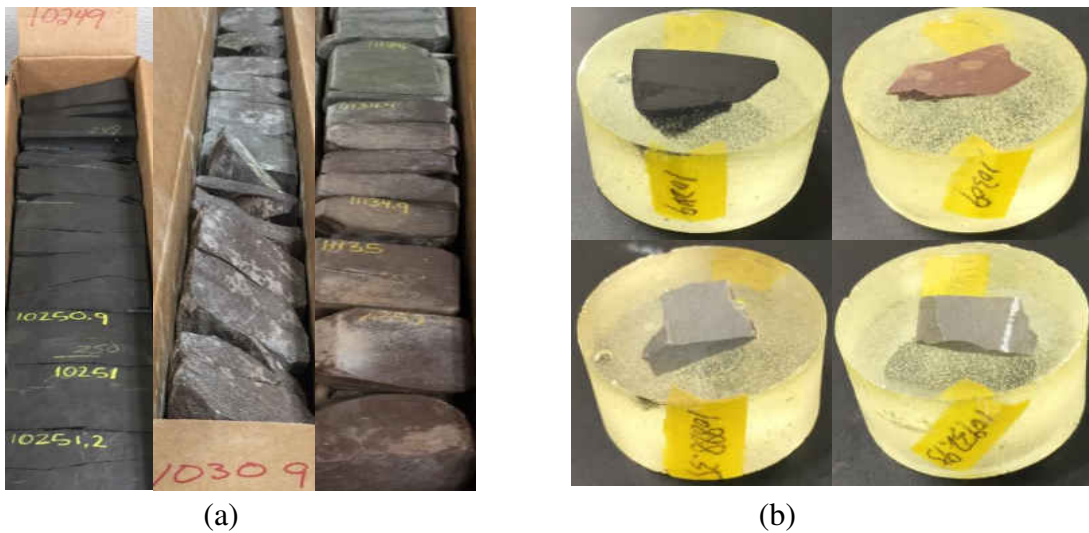


Figure 5. (a) Section of cores from Bakken for samples #2, #3, #4, #5 and (b) Sample chips in epoxy for nanoindentation tests for samples #2, #3, #4, #5

SEM on the Sample Surface

The scanning electron microscope (SEM) functions by projecting a beam of electrons through magnetic focusing lenses at a specimen and recording secondary electrons excited by the primary beam (Weinbrandt and Fatt, 1969). Here, Hitachi S-3400NH scanning electron microscope was used to observe the morphology of the Bakken samples, as shown in Figure 6.



Figure 6. Hitachi S-3400NH scanning electron microscope

Figure 7(a) shows the SEM image of the chip surface (parallel to the bedding) of sample #1 from the depth of 11135.40ft in Middle Bakken well. For the sake of characterizing the microfabric of the sample, different spots on the sample under 650 \times magnification of the sample were picked to analyze the chemical composition using IXRF EDS detector. For spot #1, it is mainly composed of element S (53.715%) and Fe (35.907%), also based on features, it is determined as pyrite. For spot #2, besides the dominant element C, minerals are mainly composed of element O (35.474%), Cl (17.86%), Si (14.206%), Na (11.579%) and K (10.207%). For spot #3, the main elements are O (36.202%), Si (32.766%) and Al (19.801%). For spot #4, minerals have the following elements: Si (56.457%) and Fe (38.248%), which are similar to spot #1. So in the image of the chip in sample #1 whose surface is parallel to the bedding of Middle Bakken, spot #1 and #4 are pyrite, spot #2 is organic matter mixed with a tiny

amount of salts and clay, spot #3 is kaolinite.

SEM-EDS analysis has been performed for sample chip whose surface is perpendicular to the bedding, as showed in Figure 7(b). We can observe a different surface features, and morphologies for two chips in one sample. As shown in Figure 7(b), bedding and micro fractures are more conspicuous. Elemental compositions of different locations were also analyzed. For spot #1, the dominant element is C. For spot #2, S (58.221%) and Fe (39.385%) are the main elements. For spot #3, it is mainly composed of element Si (57.579%) and O (41.448%). So in the image of the chip in sample #1 whose surface is perpendicular to the bedding of Middle Bakken, spot #1 is graphite, spot #2 is pyrite, spot #3 is quartz.

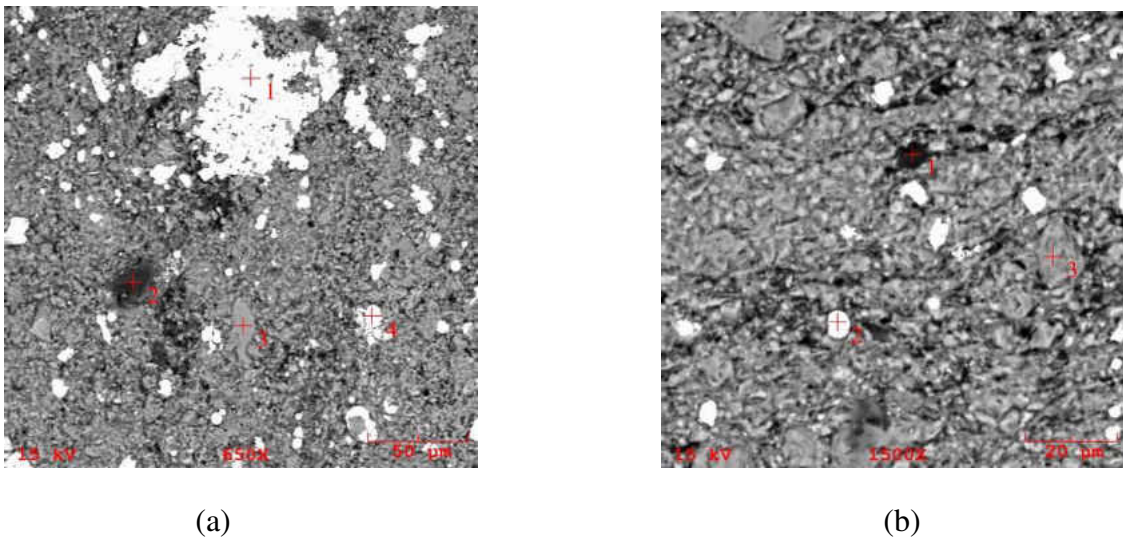


Figure 7. (a) SEM image of the chip in sample #1 whose surface is parallel to the bedding of Middle Bakken Formation and (b) SEM image of the chip in sample #1 whose surface is perpendicular to the bedding of Middle Bakken Formation

Figure 8 shows the SEM image of sample #2 from the depth of 10,888.35ft in Middle Bakken well. In order to analyze the chemical composition of the sample surface by using IXRF EDS detector, different spots under 650× magnification of the

sample were chosen. For spot #1, S (50.55%) and Fe (26.41%), it is determined to be pyrite based on the element composition. For spot #2, minerals are mainly composed of element Si (32.919%), O (27.359%), Au (13.222%), Al (10.203%), Ca (5.612%), Mg (3.379%) and K (3.649%). For spot #3, the element composition of minerals is as following: Si (48.58%), O (42.76%), Au (8.058%) and Cu (0.602%). For spot #4, the main elements of minerals are O (39.782%), Si (27.335%), Al (13.258%), Au (10.461%) and K (5.379%). According to the results of mineral composition analysis, it is estimated that substance at spot #1 is pyrite, spot #2 is organic matter mixed with clay, spot #3 is quartz, spot #4 is kaolinite.

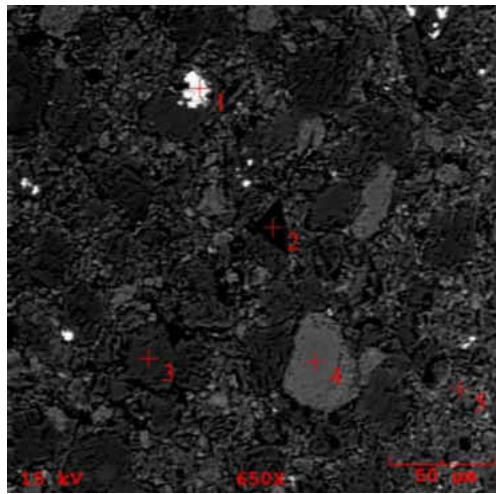


Figure 8. SEM image of sample #2 of Middle Bakken

XRD for Analyzing Chemical Element

X-rays scatter off electrons, in a process of absorption and re-admission. Diffraction is the accumulative result of the X-ray scattering of a group of electrons that are spaced in an orderly array. For an incident X-ray photon with a monochromatic wavelength λ , if the electron group interacts with the X-ray beam, a coherent wave is generated from the sample with respect to the angle θ (2θ with respect to the incident

X-ray beam) and repeated Distance d is separated. The interaction is described by Bragg's law: $n\lambda=2d\sin\theta$. The intensity of scattered X-rays is proportional to the amount of X-ray scattered electrons. (XRD Laboratory Manual, version 1.0.7). We usually use a microscope to observe small things. However, the atomic scale smaller than the light wavelength is hard to be viewed under the microscope when using the white light. At this time, it is necessary to use X-rays because they have a wavelength of 10^{-10} m, which is similar to the atomic scale.

For sample #1 from the well at depth of 11,135.4ft in Middle Bakken Formation, mineral composition analysis was carried out by using Rigaku SmartLab X-ray diffraction system, as shown in Figure 9. Table 2 shows the minerals in the rock sample #1 from Middle Bakken Formation. XRD analysis shows that the Middle Bakken rock sample #1 is mainly composed of quartz, muscovite and different types of clay minerals. X-ray diffraction patterns of sample #1 are shown in Figure 10.



Figure 9. Rigaku SmartLab X-ray diffraction system

Table 2. The weight percentage of each mineral in sample #1

Mineral	Formula	Content (%)
Quartz	SiO ₂	48.10
Dolomite	CaMg(CO ₃) ₂	3.10
Pyrite	FeS ₂	3.92
Anhydrite	Ca(SO ₄)	1.40
Anorthoclase	(Na _{0.85} K _{0.15}) (AlSi ₃ O ₈)	5.70
Chlorite	(Mg _{11.06} Fe _{0.94})(Si _{5.22} Al _{2.78})O ₂₀ (OH) ₁₆	0.68
Kaolinite	Al ₂ (Si ₂ O ₅)(OH) ₄	1.20
Muscovite	(K _{0.727} Na _{0.170} Ca _{0.011})(Al _{0.933} Fe _{0.016} Mg _{0.011}) ₂	35.90

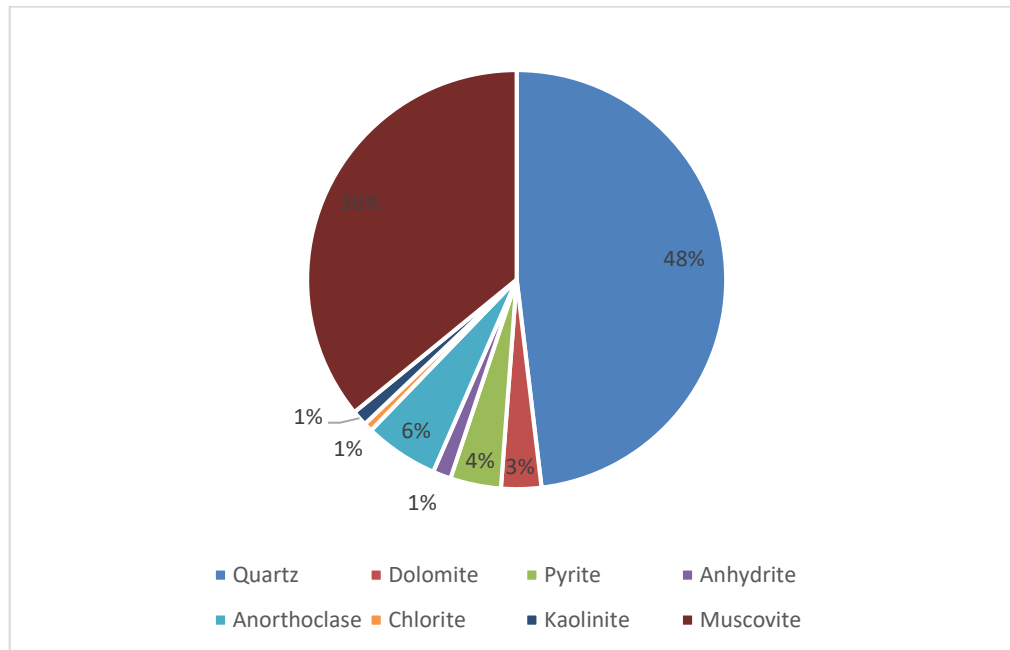


Figure 10. Profile of mineral percentage in sample #1

For sample #2 from the well at depth of 10,888.35ft in Middle Bakken

Formation, the contents of mineral phase in the rock sample are showed in Table 3. XRD analysis shows that the rock sample #2 is mainly composed of illite, quartz, dolomite and different types clay minerals. X-ray diffraction patterns of sample #2 are shown in Figure 11.

Table 3. The weight percentage of each mineral in sample #2

Mineral	Formula	Content (%)
Dolomite	$\text{CaMg}(\text{CO}_3)_2$	14.20
Quartz	SiO_2	14.90
Chlorite	$(\text{Mg}_{11.06}\text{Fe}_{0.94})(\text{Si}_{5.22}\text{Al}_{2.78})\text{O}_{20}(\text{OH})_{16}$	5.70
Sanidine	$\text{Na}_{0.56}\text{K}_{3.44}\text{Al}_4\text{Si}_{12}\text{O}_{32}$	5.73
Illite	$\text{KAl}_2(\text{Si}_3\text{Al})\text{O}_{10}(\text{OH})_2$	46.60
Pyrite	FeS_2	3.59
Albite	$\text{NaAlSi}_3\text{O}_8$	2.73
Ankerite	$\text{Ca}(\text{Fe, Mg, Mn})(\text{CO}_3)_2$	6.52

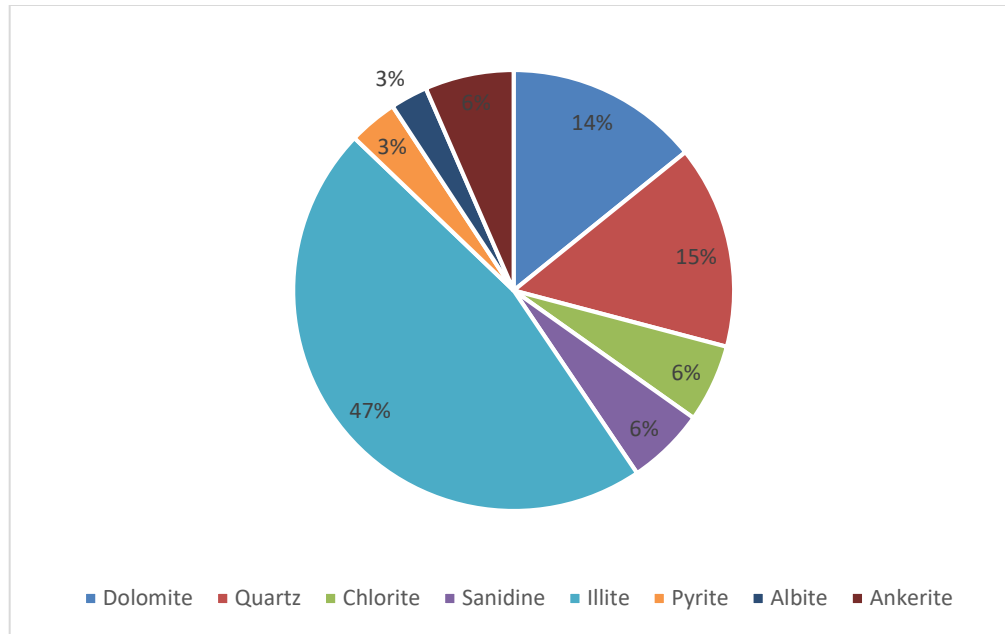


Figure 11. Profile of mineral percentage in sample #2

NANOINDENTATION TEST

The primary objective of nanoindentation is using nano technology to measure the micromechanical properties of rock materials. Nanoindentation has various modes: depth-sensing indentation, continuous-recording indentation and ultra-low-load indentation (Hay et al., 2000). A predominant influence of nanoindentation experiment is the flatness of the rock samples related to the precision of the experiment. The indenter of the equipment moved slowly towards to the surface of the rock sample, exerting a force on the sample surface after contacting with the sample. Force as low as 1nN can be applied and displacements as small as 0.1nm can be measured (Hay et al., 2000). When the force becomes maximum on the sample, the displacement reaches the peak. All the forces changed with displacement were recorded by the equipment, which is called Hysitron TI-700 ubi nanomechanical indenter showed in Figure 12.



Figure 12. Hysitron TI-700 ubi nano-mechanical indenter

Figure 13 represents load-displacement curve obtained from nanoindentation testing. The plot displays load along the y-axis and displacement along the x-axis. It shows the peak load P_{\max} and maximum displacement depth h_{\max} . All the calculations of Young's modulus and hardness are carried out at peak load (Shukla et al., 2013). The slope of the unloading process represents the contact stiffness of the material, S (Equation 1) (Oliver and Pharr, 1992):

$$S = \frac{dP}{dh} = \beta \frac{2}{\sqrt{\pi}} E_r \sqrt{A} \quad (1)$$

Where S is the slope of the unloading curve, E_r is the reduced Young's modulus of the Berkovich diamond indenter tip, A is the contact area between the tip and the sample, β is a factor equals to 1.034 related to the shape of Berkovich indenter.

Material with high stiffness has a large slope value. The contact stiffness can be tested by equipment via using the slope of unloading. Then using Equation 1 to

calculate the reduced Young's modulus E_r , calculating Young's modulus through Equation 2 (Oliver and Pharr, 1992):

$$\frac{1}{E_r} = \frac{1-\nu^2}{E} + \frac{1-\nu_i^2}{E_i} \quad (2)$$

Where ν and E are Poisson's ratio and Young's modulus of the sample, ν_i and E_i are Poisson's ratio and Young's modulus of the tip, respectively. The Poisson's ratio and Young's modulus of the Berkovich diamond tip used in the nanoindentation test are 0.07 and 1141GPa, respectively.

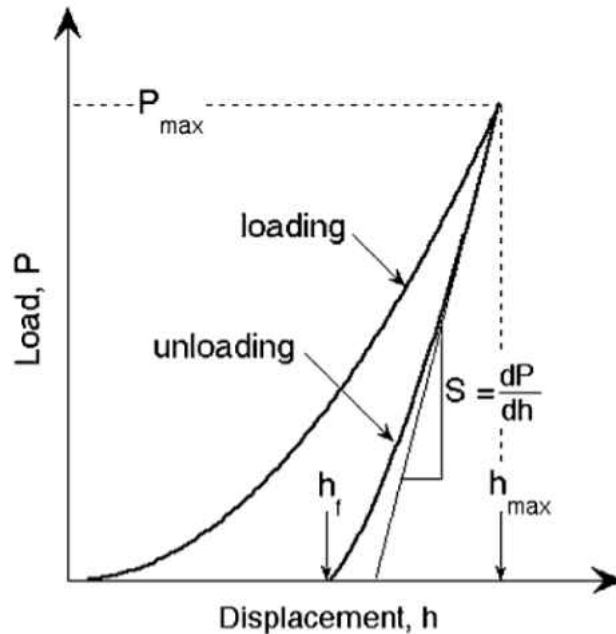


Figure 13. The curve of loading-unloading in the process of indentation (Oliver and Pharr, 2004)

Hardness can be used to express the extent of resistance from the force, which is equal to the ratio of the maximum peak load by the indenter and contact area of the tip.

Micromechanical properties including hardness, Young's modulus, and penetration depth were determined by nanoindentation performed on Bakken specimens. Each sample has 64 indentations which are enough to get rock properties in

experiments. Four arrays of 4×4 indentations were made in different locations on the sample surface and the average Young's modulus and hardness of these 64 indentations can be a presentative value for sample properties. Figure 14 shows an array of 4×4 indentations on rock sample.

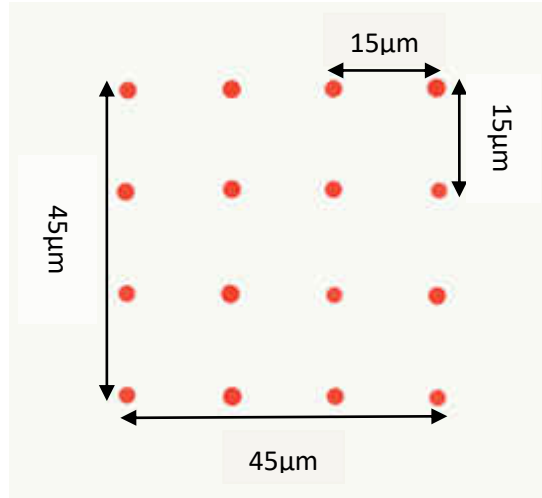


Figure 14. An array of 4×4 indentations on the rock sample

The results of nanoindentation test for the sample with indentation perpendicular to the bedding of Middle Bakken, and sample with indentation parallel to the bedding are shown in following figures. For the rock chip in sample #1 whose indentations are parallel to the bedding of Middle Bakken Formation, the Young's modulus ranges from 14.969 to 152.303GPa, and the hardness ranges from 0.384 to 11.353GPa. For the rock chip whose indentations are perpendicular to the bedding of Middle Bakken Formation, the Young's modulus ranges from 11.700 to 123.675GPa, and the hardness ranges from 0.457 to 8.378GPa. The difference of properties in the sample is pretty much due to the heterogeneity in the sample. These phenomena also can be proved by SEM images of the sample surface in Figure 7. Because the sample is heterogeneous, more indentations we have is more beneficial to the accuracy of

experiments.

The hardness as a function of Young's modulus for perpendicular and parallel indentations on Middle Bakken rock samples are plotted in Figure 15 and 16, respectively. The data of hardness versus Young's modulus lie along a straight line with some data points scattering away from a linear relationship.

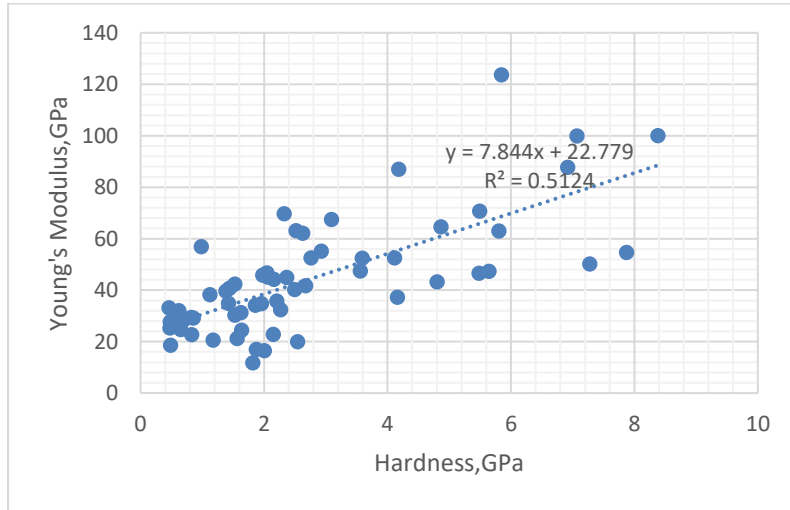


Figure 15. Young's modulus vs. hardness for all indentations on sample #1 (Indentations perpendicular to the bedding of Middle Bakken)

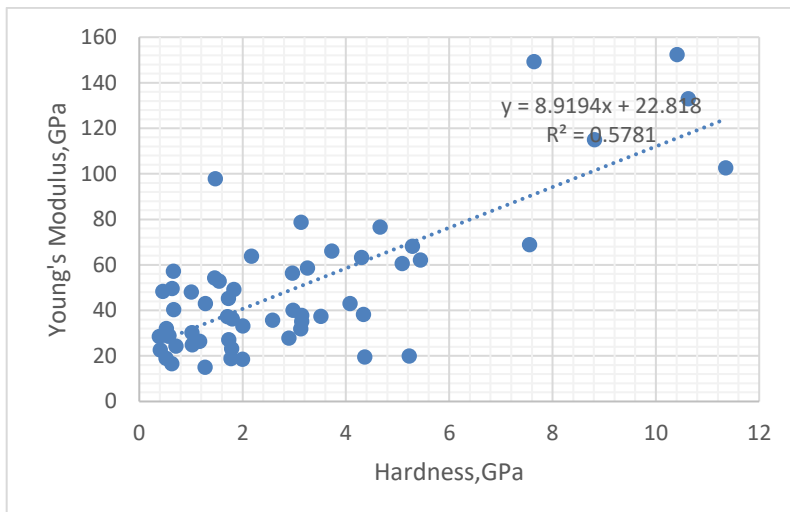


Figure 16. Young's modulus vs. hardness for all indentations on sample #1 (Indentations parallel to the bedding of Middle Bakken)

The Continuous Stiffness Measurement (CSM) method was used to determine the variation of the static elastic modulus and hardness versus penetration depth. Figures 17 and 18 illustrate the average Young's modulus as an expression of indentation numbers for perpendicular indentations and parallel indentations, respectively. For the rock chip whose indentations are perpendicular to the bedding of Middle Bakken in sample #1, it can be seen in Figure 17 that the average Young's modulus value becomes a steady value after the number of indentations overpass 30. The average Young's modulus value is about 45GPa. For the rock chip whose indentations are parallel to the bedding of Middle Bakke in sample #1, the average Young's modulus is about 50GPa as shown in Figure 18.

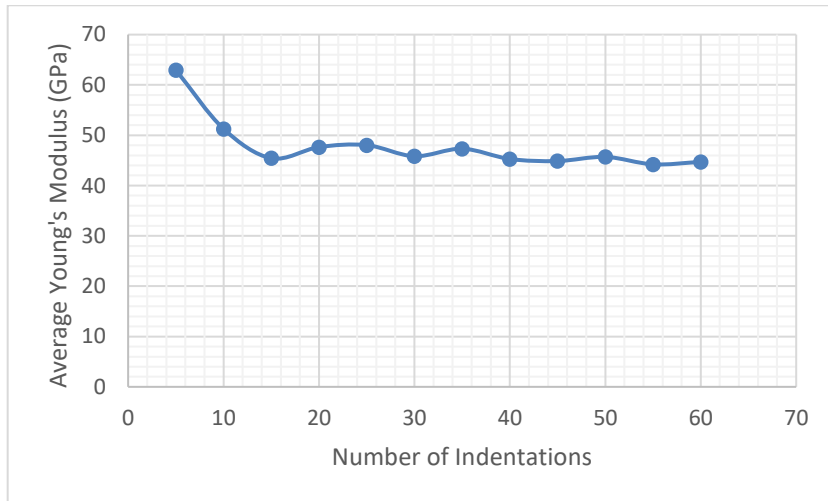


Figure 17. Average Young's modulus vs. number of indentations on sample #1 (Indentations perpendicular to the bedding of Middle Bakken)

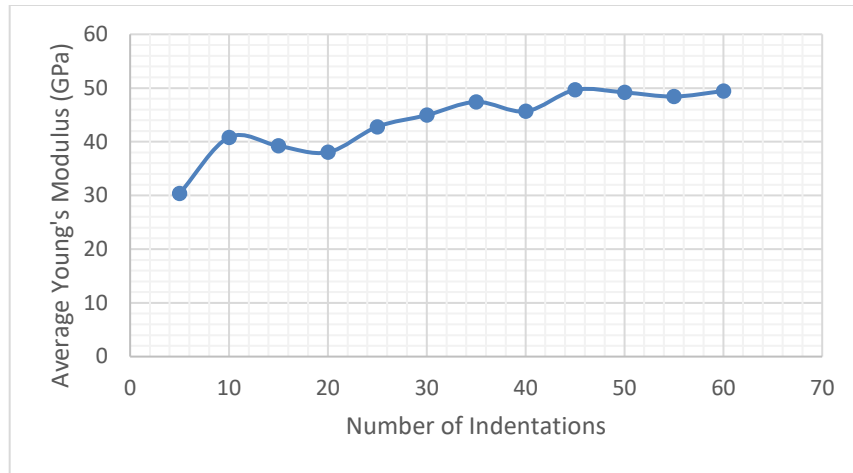


Figure 18. Average Young's modulus vs. number of indentations on sample #1 (Indentations parallel to the bedding of Middle Bakken)

Figures 19 and 20 show the relationship between the hardness and number of indentations at the nano scale for indentations perpendicular and parallel to the bedding of Middle Bakken, respectively. The hardness as a function of penetration depth behaves similarly in two samples, indicating that similar indentation-induced deformation mechanism is prevailing in samples studied (Shengrui et al., 2013). The initial sharp increase in hardness at small penetration depth is usually attributed to the transition from purely elastic to elastic/plastic contact (Almeida et al., 2008). Pang et al (2003) reported that only under the condition of a fully developed plastic zone does the mean contact pressure represent the hardness. As can be seen in Figures 19 and 20, for the rock chip whose indentations are perpendicular to the bedding of Middle Bakken in the sample #1, the average hardness becomes an approximate steady value of 3.0GPa after 45 indentations; for the rock chip whose indentations are parallel to the bedding of Middle Bakken in the sample #1, the average hardness becomes an approximate steady value of 3.0GPa after 50 indentations.

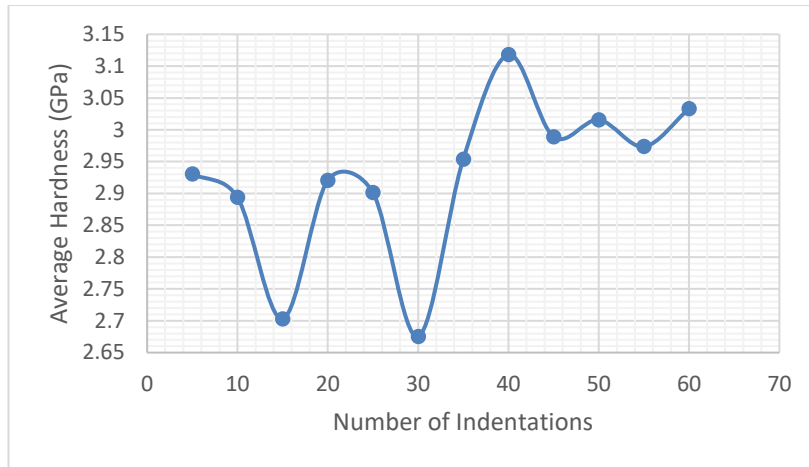


Figure 19. Average hardness vs. number of indentations on sample #1 (Indentations perpendicular to the bedding of Middle Bakken)

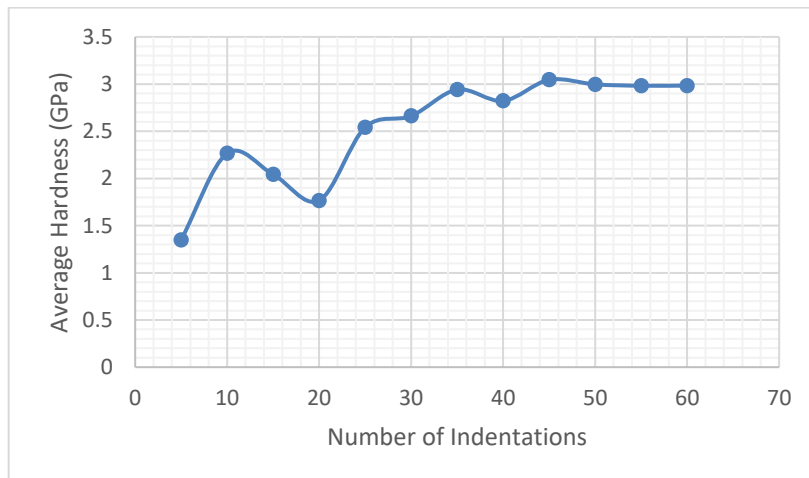


Figure 20. Average hardness vs. number of indentations on sample #1 (Indentations parallel to the bedding of Middle Bakken)

From nanoindentation tests, the results of experiments for rock samples show different elastic properties in Bakken formation. For the sample #2 chosen from the depth of 10,888.35ft in the well called Chruszch 43X-29F of Middle Bakken, the Young's modulus ranges from 16.906 to 146.214GPa. Due to heterogeneity on the sample surface which can be proved by SEM test shown in Figure 8, the difference of the mechanical property in the same sample is quite large. Figure 21 shows the

relationship between Young's modulus and the number of indentations for the sample #2. After the number of indentations is over 50, the average Young's modulus maintains a steady value of around 78GPa.

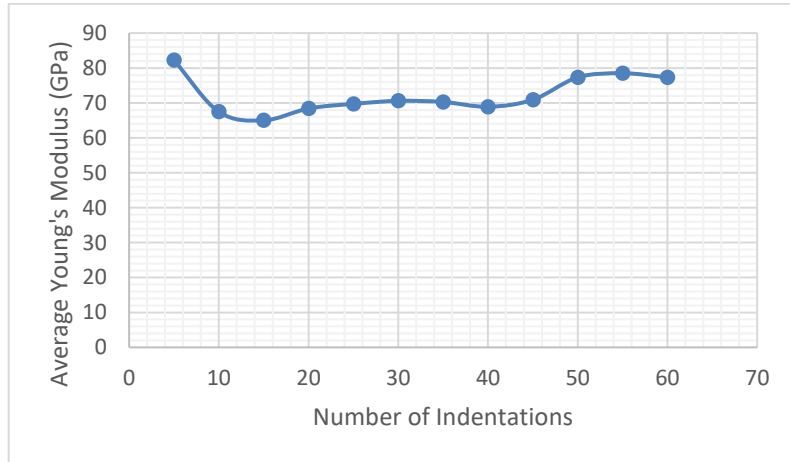


Figure 21. Average Young's modulus vs. number of indentations on sample #2 of Middle Bakken

Figure 22 shows the relationship between the average hardness and number of indentations. The initial sharp in hardness at small penetration depth is usually attributed to the transition from purely elastic to elastic/plastic contact. It eventually reaches a constant value at the indentation numbers of approximately larger than 35. The results indicate that the sample demonstrates an average hardness of about 5.1GPa.

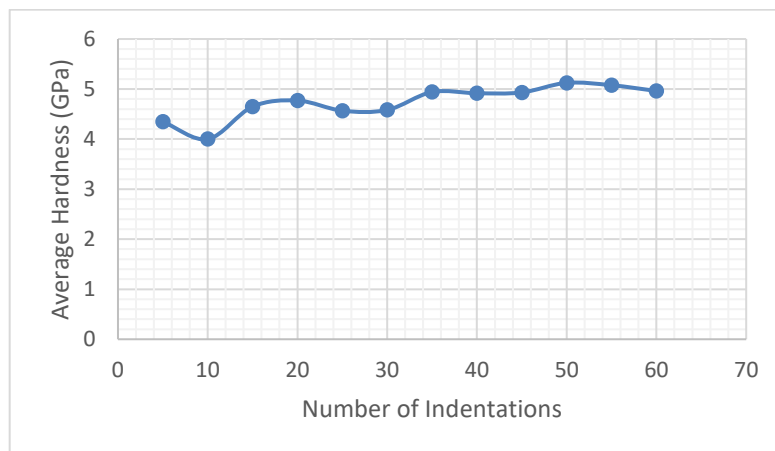


Figure 22. Average hardness vs. number of indentations on sample #2 of Middle Bakken

Figure 23 shows Young's modulus of the sample as a function of its hardness. The relationship between Young's modulus and hardness represents a straight line. The data of hardness versus Young's modulus lie along a straight line with some data points scattering away from a linear relationship. When hardness is below 10GPa, the points of Young's modulus are densely distributed on both sides of the trend line. The linear equation of the trend is listed in Figure 23.

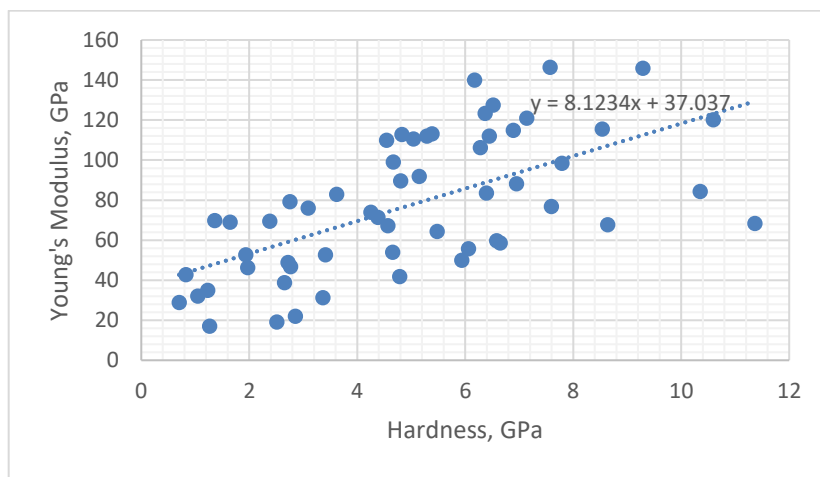


Figure 23. Young's modulus vs. hardness for all indentations on sample #2 of Middle Bakken

The Young's modulus of the sample #3 from the depth of 10,932.95ft in the same well called Chruszch 43X-29F of Lower Bakken has a close range as the sample from the depth of 10,888.35ft. From nanoindentation data, it can be known that Young's modulus of the sample from the depth of 10,932.95ft range from 11.571 to 184.823GPa and have an average value of 75GPa. The hardness ranges from 0.473 to 14.464GPa with an average value of 4.8GPa. The Young's modulus of the samples from a different well called Pumpkin 148-93-14C-13H TF of Bakken has a different

range. The sample #4 from the depth of 10,249ft in the well Pumpkin 148-93-14C-13H TF has a range of Young's modulus from 8.334 to 88.280GPa and have an average value of 38GPa. The Young's modulus of sample #5 from the depth of 10,309ft in the well Pumpkin 148-93-14C-13H TF has a range from 14.879 to 104.333GPa, and the average value is 51GPa. The hardness of sample #4 and #5 from the depth of 10,249ft and 10,309ft in the well Pumpkin 148-93-14C-13H TF ranges from 0.108 to 12.085GPa and 0.463 to 8.122GPa, respectively. And the average hardness value for sample #4 and #5 are 3.2 and 2.4GPa. All the measured average Young's modulus and hardness are listed in Appendix C for all the samples.

CHAPTER IV

SIMULATION OF ROCK PROPERTIES

Introduction of Finite Element Analysis

Finite Element Method (FEM) is sometimes referred to as Finite Element Analysis (FEA), a mathematical approximation method to simulate real physical systems which has definite geometry and load conditions. This method provides an analytical model which is able to resolve many of the variables encountered in rock mechanics (Anderson and Dodd, 1966). Commercial FEM software ANSYS 18.1 was used to build a model to portray a rock mass. Then using simple and interactive elements, such as units, to approximate a real system of infinite unknowns with a finite number of unknowns.

The main idea of FEM is dividing the continuous structure into a finite number of units, and setting a limited number of nodes in each unit, then treating the continuum as a collection of units connected only at the nodes. The node value of the selected field function is regarded as the basic unknown quantity, and an approximate interpolation function is assumed in each unit to represent the distribution law of the field function in the unit. Next, using variational principle in mechanics to establish finite element equations which are used to find the unknowns of nodes. Through these equations, the problem of finite degrees of freedom in a continuous domain can be transformed into a finite degree of freedom (DOF) problem in the discrete domain. In which, DOF is used to describe the response characteristics of a physical field. Equations predicting the

behavior of each finite element are established, and then the equations for all elements are solved simultaneously (Anderson and Dodd, 1966).

In short, the boundary value problem with finite degrees of freedom is a mathematical program in which one or more dependent variables must satisfy the differential equation anywhere within the known domain of the independent variable and satisfy certain conditions at the boundaries of the domain. The boundary value problem is also called a field problem. This area is an area of interest and usually represents a physical structure. The field variable is the dependent variable of interest controlled by a differential equation. The boundary condition is the specified value of this field. Depending on the type of physical problem being analyzed, field variables which are also called DOF may include physical displacement, temperature, pressure, electrical and magnetic potential.

Application of ANSYS on Shale

Nanoindentation tests are commonly used to evaluate the rock's response. As shown in Figure 24, consider a rock surface that is indented by a pyramidal indenter. Then the load is removed from the indenter, the material attempts to regain its original shape, but can only get a certain degree of recovery prevented from the plastic deformation (h_f is the depth of residual impression) (Kouqi, 2017). The angle between the indenter and the axis of rotation is 68° . Rock sample #1 with a yield strength of 550MPa was chosen as an example for programming in Appendix C. In simulation part, two samples with different yield strength were used, which is shown in Table 4. Table 4 presents Young's modulus and Poisson's ratio of the constituent materials. The value of Young's modulus of samples was selected from indentations according to the average

Young's modulus listed in Appendix B.

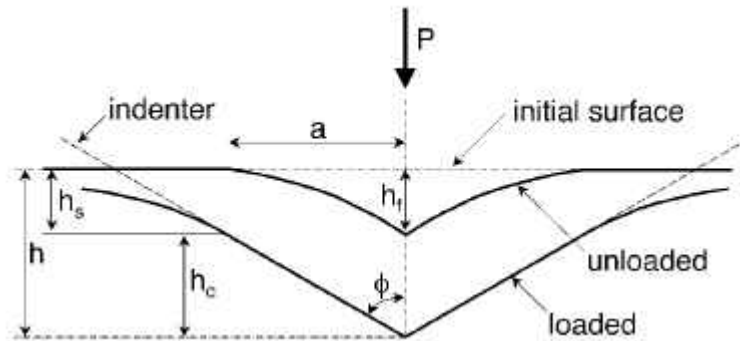


Figure 24. Schematic illustration of nanoindentation process (Oliver and Pharr, 1992)

In order to correctly simulate the indentation phenomenon, contact analysis was used. For this purpose, the contact element was placed along the top surface of the rock and the target element was used along the bottom surface of the indenter. The indentation was simulated by applying displacement boundary conditions in the y-direction along the nodes of the rock sample. Thus, the top surface of the rock was pressed against the bottom surface of the indenter so that the contact element was applied to the target element. Assume that the contact is frictionless. The indentation was performed using several displacement steps, each writing a load step file. to simulate loading and unloading process. The displacement steps for loading and unloading are 10.35 and 5.00nm. Rock sample #1 with the yield strength of 550MPa was modeled using PLANE 183 elements. All the nodes on the y-axis could only have the displacement in the y-direction. The upper surface of the indenter was limited in all directions. The goal is to obtain the indentation and force response of the rock.

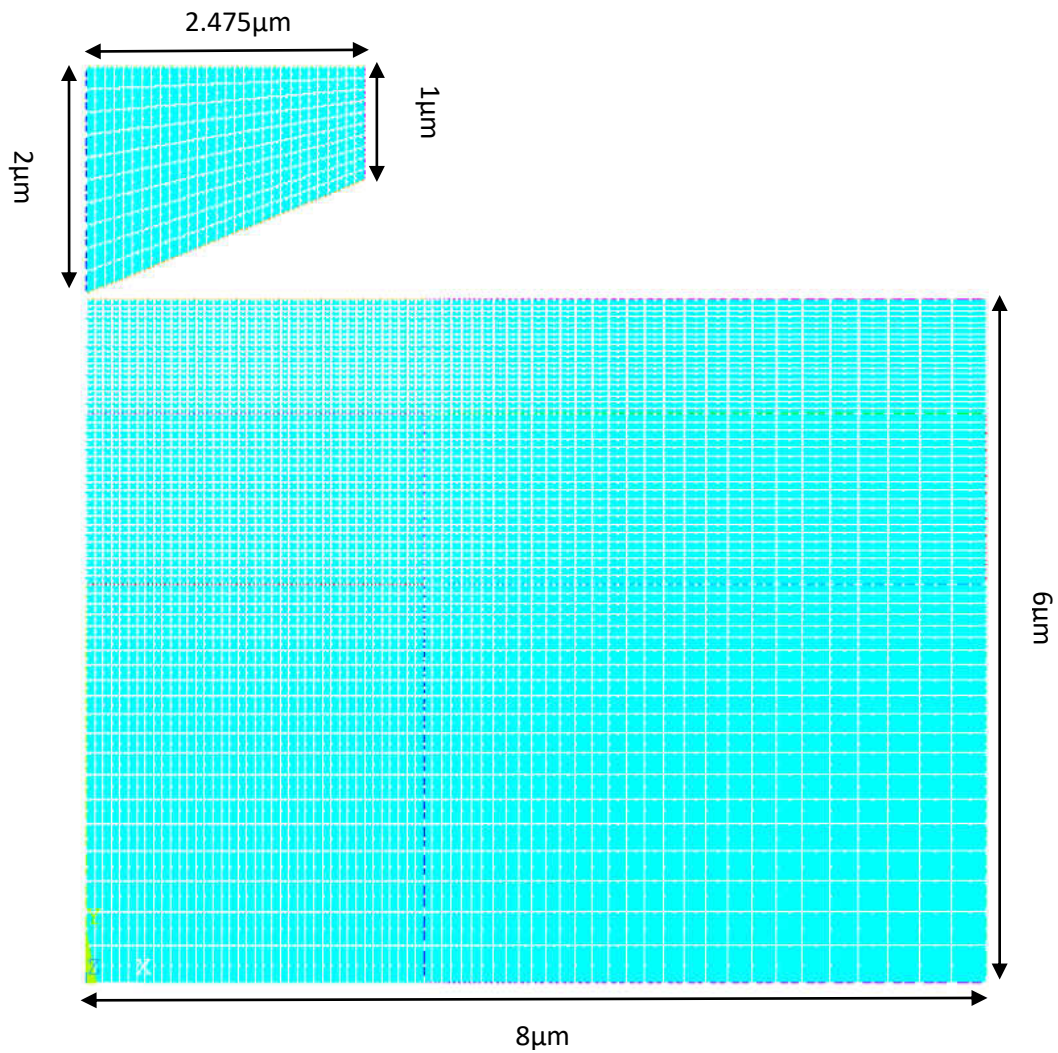
Table 4. Material properties used in numerical simulation

Material	Young's Modulus (GPa)	Poisson's Ratio	Yield Strength (MPa)
Sample #1	52.79	0.23	550.00
Sample #2	82.75	0.25	1,450.00
Diamond Indenter	1,141.00	0.07	

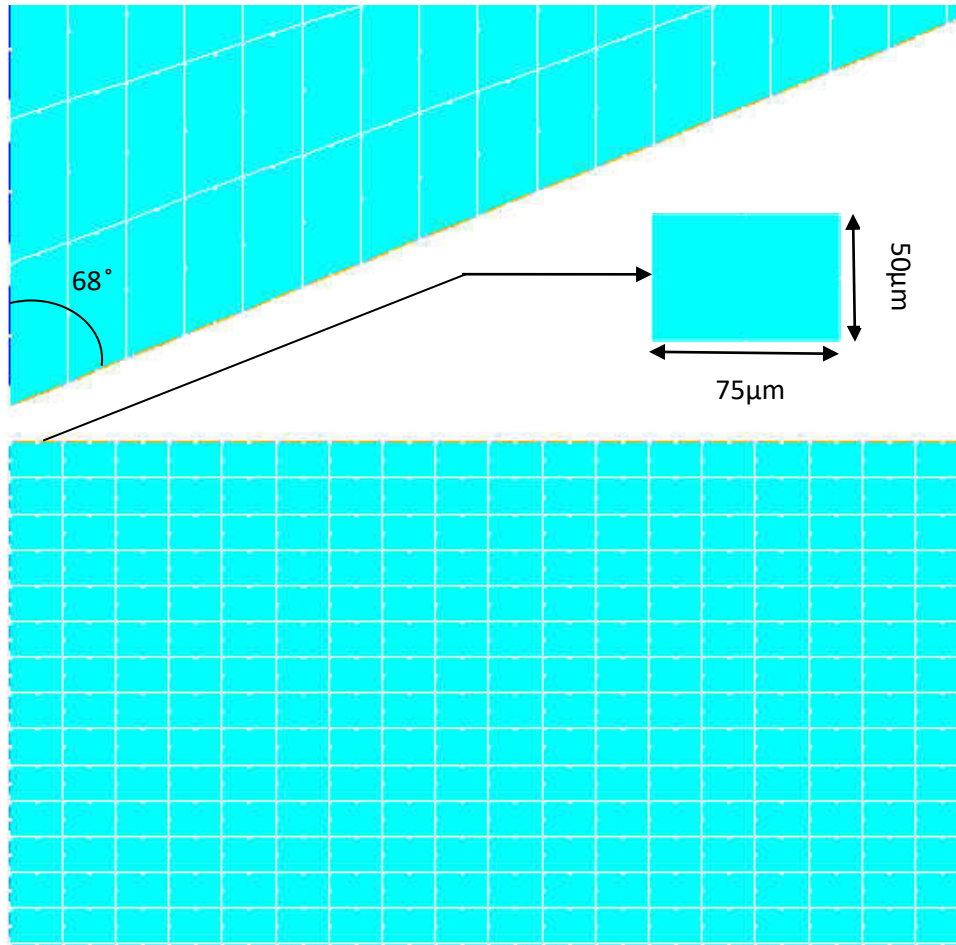
Building of Geometry Model

Geometry model was mainly composed of the indenter and the rock. In order to create a solid model, starting with the key points, then lines, regions. The elastic complete plastic behavior of the rock was combined using a bilinear isotropy hardening rule and a tangent modulus of zero (Erdogan, 2005). After inputting preprocessing program from Appendix C in File Menu of ANSYS Mechanical APDL 18.1, the model was generated in the x-y plane and meshed using two-dimensional elements. Figure 25(a) shows an isometric view of the grid used in this analysis and Figure 25(b) demonstrates the detailed meshing of rock sample near contact area. As for the semi-rock mass in Figure 25(a), a total mesh area of $8\mu\text{m}$ long and $6\mu\text{m}$ wide is enough to eliminate the effect of boundary, which represents the cylindrical rock sample in the model has a radius of $8\mu\text{m}$ with the thickness of $6\mu\text{m}$. Also, the indenter in the model has a radius of $2.475\mu\text{m}$. Most of the deformation occurs immediately under the indented area, the highest mesh density was employed around the indenter tip (Ban et al., 2014). Each meshing unit close to the contact surface between the rock and nano-indenter has a size of $75\text{nm} \times 50\text{nm}$. In order to reduce the computational time, the size of meshing units which are further away from the contact area is significantly larger

than the units close to the nano-indenter. After finishing the building of geometry model and meshing, the bottom surface of indenter and rock sample surface was designated as target surface and contact surface, respectively. So the target surface and contact surface formed a contact pair. The contact surface would be moved into the target surface to simulate the nanoindentation process. Also, the top surface of the indenter was restrained in all directions according to the indenting process.



(a)



(b)

Figure 25. (a) Isometric view of the finite element mesh used for the nanoindentation simulation and (b) Detailed meshing near contact area

Solution

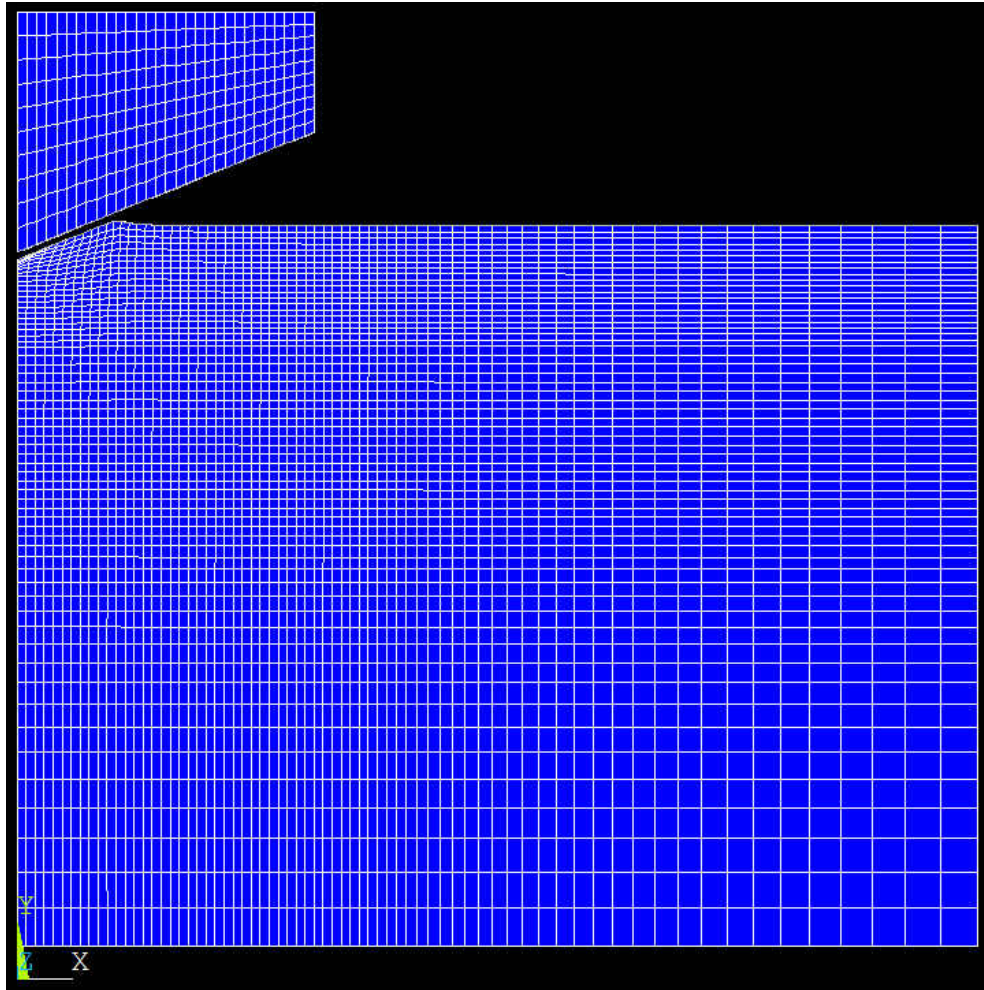
The indentation was simulated by specifying the process of the rock moving forward to the indenter in the y-direction. This shift was applied in increments of 10.35nm for the loading phase and its value was stored in the array parameter DIS. Array parameters were created using the *DIM command and the array size was 57. The 57 steps represent the total process of loading and unloading. The first 36 steps of the array correspond to the loading process. During the loading process, the rock

surface moved forward to the indenter in y-direction displacement until the indentation depth became maximum. The following 21 steps were the unloading process. Each step has a constant unloading depth and these final 21 steps constituted the unloading displacement. All the records of loading and unloading displacement were saved in DIS command through the do loop. The nonlinear geometry effect and automatic time stepping were both on. Then to control solution data written to the database and control solution printout. Using the full Newton-Raphson method without the adaptive fallback option (NROPT command) (Erdogan, 2005). The maximum numbers of substeps cannot be too small in order to solve nonlinear large strain problems (Chi, 2009). Therefore, using the NEQIT command to set the maximum number of balance iterations per substep to 100. Here, input Solution command from Appendix C in File Menu of ANSYS Mechanical APDL 18.1 was used to achieve the commands above.

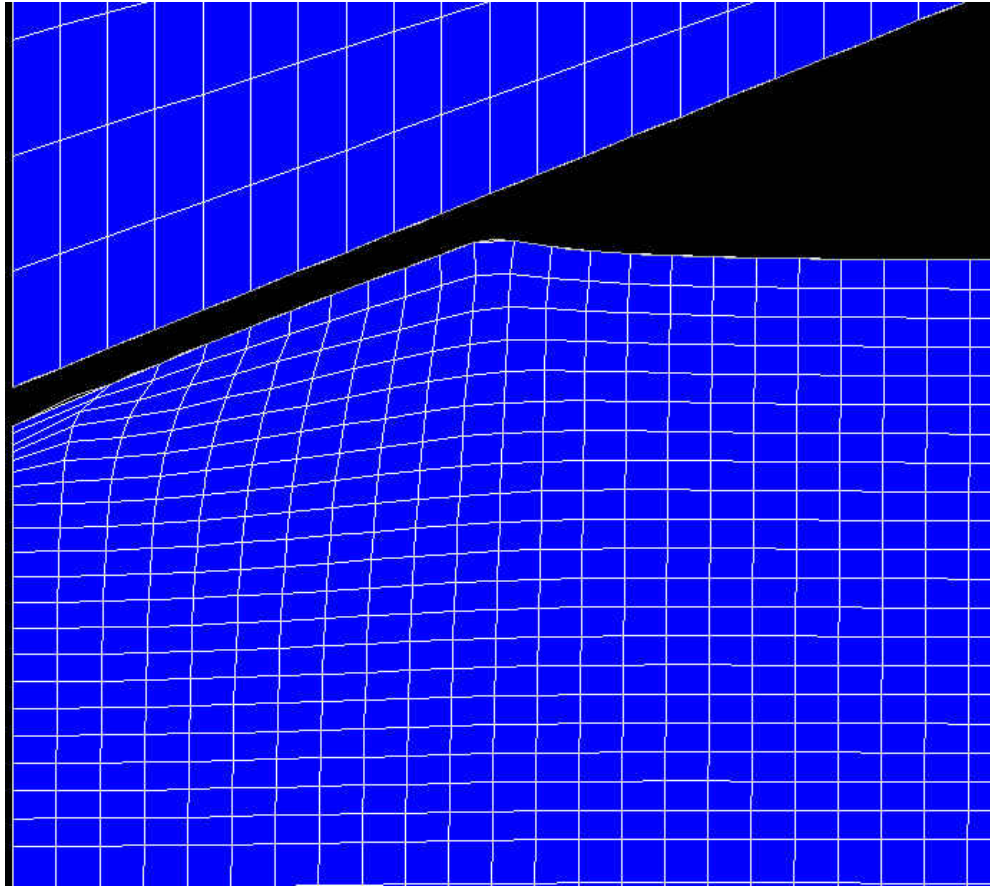
Postprocessing

To obtain the relationship of load force and indentation depth on the rock surface, using ANSYS Mechanical APDL 18.1 to read the postprocessing programming in Appendix C. The load force and indentation depth values for each load step were extracted within the do loop. The results corresponding to the load step were read via the SET command. In the programming, selected nodes were used to explore the load force with the indentation depth. The SUM command was utilized to initialize the original total reaction force and then record the current total reaction force. Due to the force balance, this amount must be the same as the force exerted by the indenter on the top of the rock. For each load step, the indentation depth applied in the array parameter DIS and the corresponding total reaction force stored in the parameter SUM were

written to the file NANO.OUT using the combined /OUTPUT and *VWRITE commands (Erdogan, 2005). Figure 26(a) and (b) shows the deformation of sample #1 after loading and detailed deformation near the contact area, respectively and Figure 27 shows the von Mises stress distribution of the rock sample #1.



(a)



(b)

Figure 26. (a) Image of deformed shape after loading in simulation and (b) Detailed deformation near contact area

The von Mises stress yield criterion can also be called as the von Mises stress. It suggests the yielding of a ductile material. The material will start yielding when its von Mises stress reaches a critical value (yield strength) (Chi 2009). In Figure 26, the maximum von Mises stress in the rock sample #1 is 558.565MPa when the yield strength is 550MPa. Due to the effect of pile up showed in Figure 26(b), another maximum von Mises stress of rock sample exists at the right side of indenter tip, besides the common one under the indenter tip.

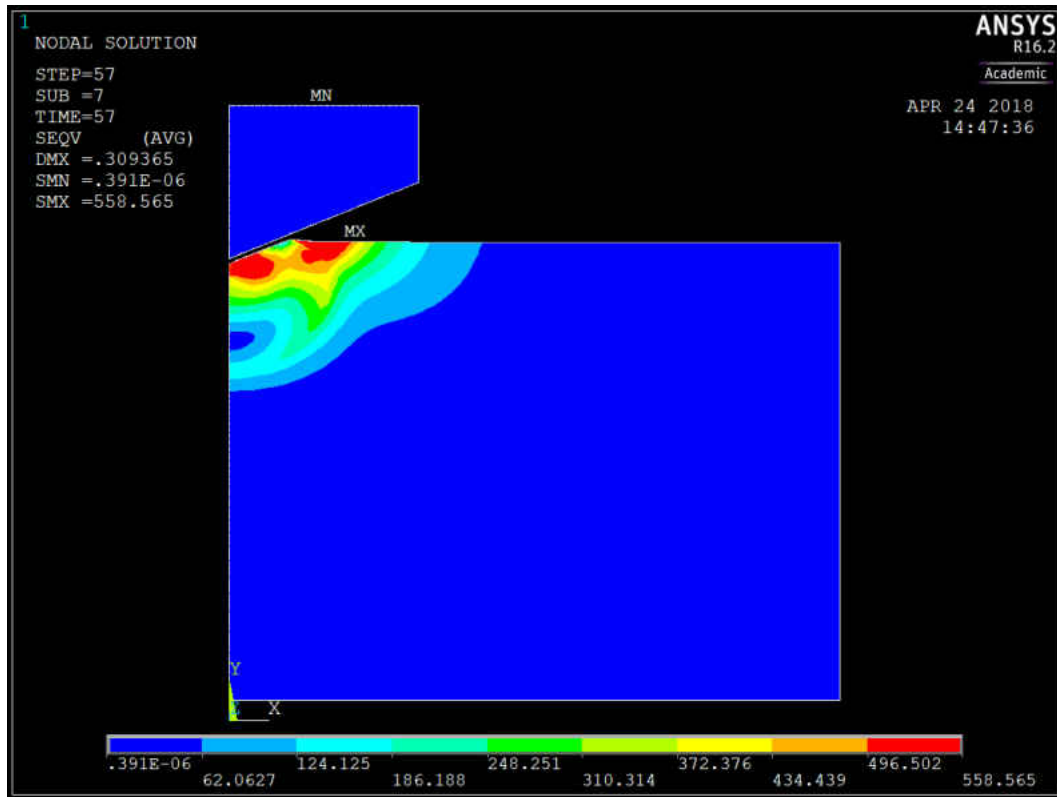


Figure 27. Von Mises stress distribution of rock sample #1

Results of Simulation and Analysis

After running the program to simulate the process of nanoindentation tests, we can get the relationship of displacement and force for loading and unloading process. From the slope of the unloading curve, the micromechanical property such as Young's modulus can be calculated. Figure 28 shows a curve of loading and unloading experimental process when Young's modulus is 52.794GPa for the sample #1 from depth 11,135.40ft of LINSETH 13-12HW in Middle Bakken. From the Figure 28, the maximum depth of indentation also called total loading displacement is 307.3nm. Actually, the maximum force applied on the sample surface is 2,999.6 μ N. After loading and holding process, the displacement of unloading process is 307.3nm.

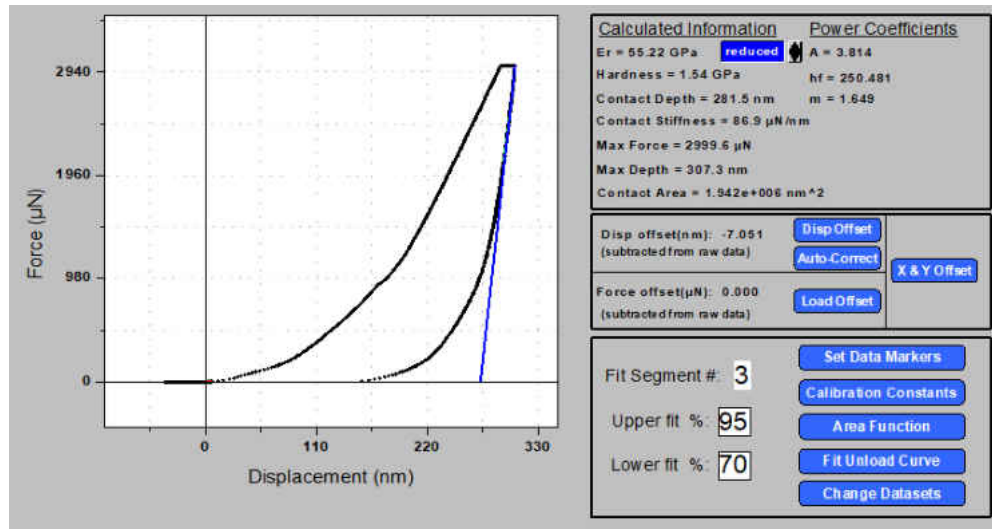


Figure 28. Experimental curve of nanoindentation process for sample #1

In order to compare with the experimental result of nanoindentation, the ANSYS Mechanical APDL 18.1 software was used to simulate the test process with setting the same rock properties such as Poisson's ratio, Young's modulus, yield strength and exert similar maximum force 3015.6µm on the sample #1. Figure 29 was produced by the data chart in the NANO.OUT document which created after postprocessing.

As for the simulation result of sample #1, the force is very close to the experimental data in the loading part. The slope of unloading part is 93.95µN/nm, which is not far from the contact stiffness of 86.9µN/nm in experimental data. Although the simulation is the best fit with the experiment, the final stage of unloading part in the simulation doesn't fit very well when the displacement is less than 290nm, which implies that some other factors may need to be considered in the model for better consistency.

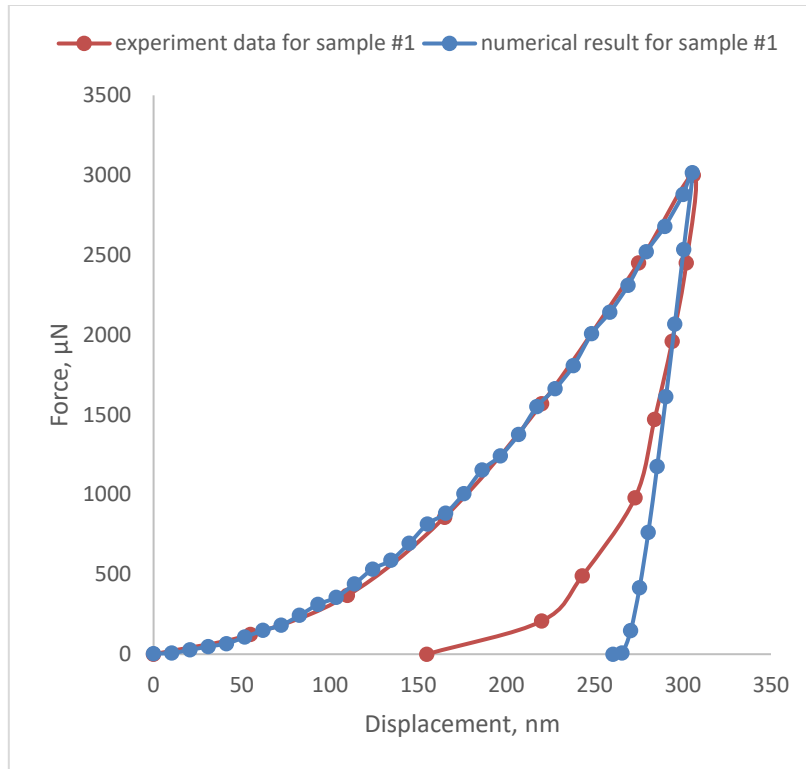


Figure 29. The relationship of displacement and force in simulation for sample #1

As for sample #2 from 10,888.35ft of Chruszch 43-29F in Middle Bakken, Young's modulus used in the simulation is 82.75GPa, the maximum force exerted on the sample#2 is 3,017.9μN. The total displacement of loading process is 216.0nm (Figure 30), the contact stiffness is 85.0μN/nm in the nanoindentation experiment.

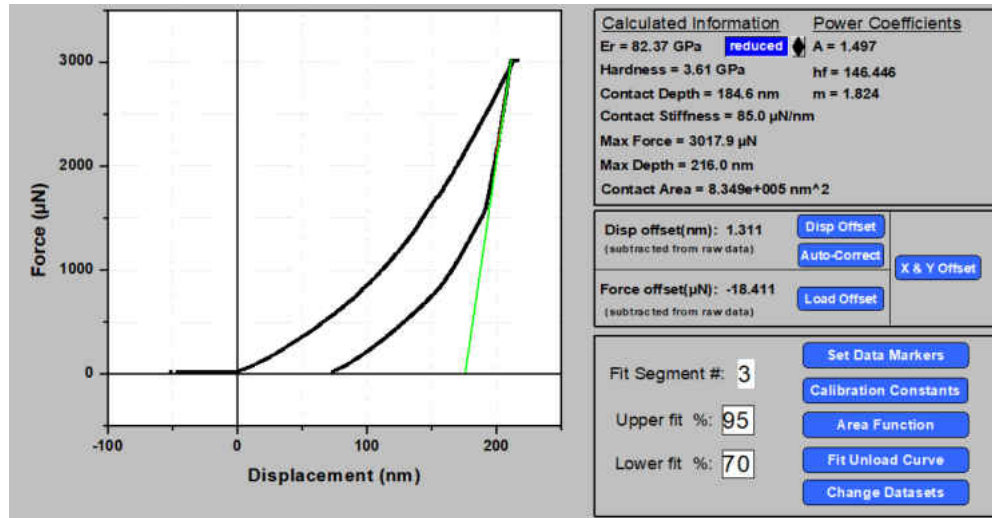


Figure 30. Experimental curve of nanoindentation process for sample #2

In order to compare with the experiment data for sample #2 when the Young's modulus is 82.750GPa, the yield strength of sample #2 was set as 1,450MPa, the loading and unloading depth was set as 7.66 and 5.00nm. From the numerical results in Figure 31, we can see when the loading displacement is similar to the experiment, the maximum force exerted on the sample #2 in the simulation is 2,990.4µN which is a little smaller than maximum force in the experiment. The loading force in the simulation is a little smaller when the loading displacement is less than 160nm but larger than the experiment when the displacement is over 160nm. In the unloading results of numerical simulation, the slope of the unloading curve is 87.17µN/nm, which is very close to the contact stiffness of 85.0µN/nm in the experiment data. Because Young's modulus can be calculated through contact stiffness, Young's modulus from the simulation result is similar to the value in the experiment, which means the results of the experiment and numerical simulation in sample #2 are identical, basically.

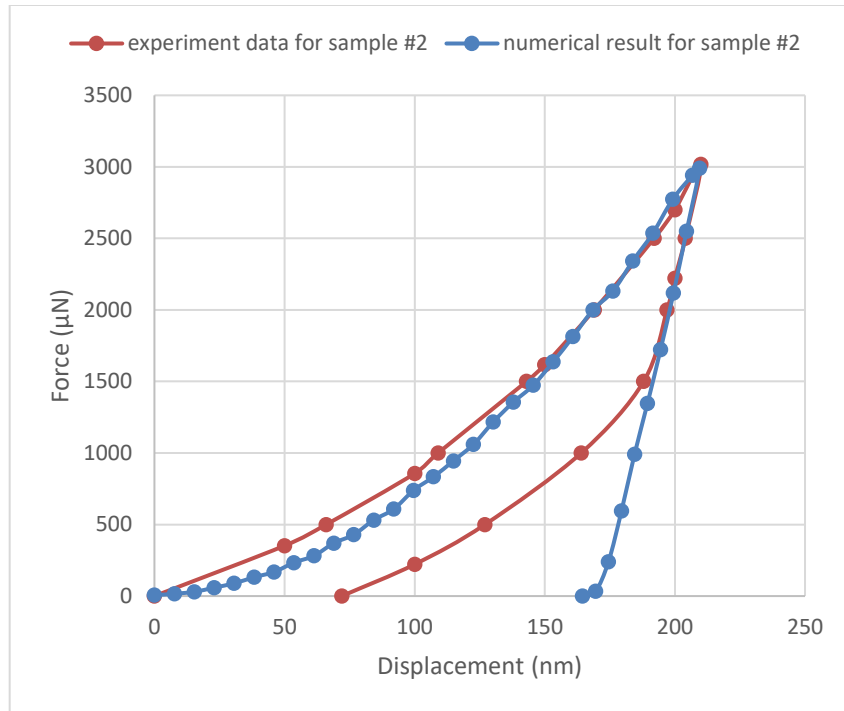


Figure 31. The relationship of displacement and force in simulation for sample #2

CHAPTER V

CONCLUSIONS

During nanoindentation tests, different rock samples have a different range of Young's modulus and hardness due to heterogeneity which can be proved in SEM. For the rock chips in the same depth of same well from Middle Bakken, although the directions to the formation bedding are different, Young's modulus and hardness are still very close. The result can be proved by the rock chips which are parallel and perpendicular to the bedding of Middle Bakken of sample #1.

Comparing samples #2 with #3, which are from the same well but from Middle and Lower Bakken respectively, the differences of Young's modulus and hardness are not significant. Also, the difference of rock properties depends on the variation of depth.

Comparing samples #4 with #5, although both are from the same well of Lower Bakken, their mechanical properties still have some difference. The average Young's modulus for sample #4 and #5 is 38 and 51GPa respectively. Meanwhile, the average hardness is 3.2 for sample #4 and 2.4GPa for sample #5.

Combing the results of XRD and nanoindentation results for samples #1 and #2, sample #1 is mainly composed of quartz, muscovite and anorthoclase but sample #2 is mainly composed of illite, quartz and dolomite. The average Young's modulus for samples #1 and #2 are 50 and 78GPa, respectively. And the hardness of samples #1 and #2 is 3.0 and 5.1GPa, respectively. That means diverse mineral composition may cause varied rock properties.

In the process of simulation, the yield strength of rock sample has an effect on simulation results of nanoindentation. The results of numerical simulation in samples #1 and #2 are consistent with the experiment, basically. The coincidence between the experiment and numerical simulation verified the accuracy of both the test and simulation method.

While more testing, data analysis, and extended-range model functions are needed to confirm the methodology presented in the study, this means that the integrated experiment-numerical effort can at least partially overcome the drawbacks of some conventional test analysis methods.

Although the experiment-numerical method has a lot of benefits when measuring the rock properties, it still has the improvement space to take into the consideration of some factors, such as scale effect etc. Further investigation and studies are recommended when building the modeling of rock samples.

APPENDICES

Appendix A

Core Section Descriptions

The cores used in the experiments were obtained from the Wilson M. Laird Core and Sample Library, Grand Forks, ND.

Well A: LINSETH 13-12HW, WPX Energy Williston LLC

11110 – 11140ft Shale: Black, brownish black, blocky, platy, fissile, angular, smooth, carbonaceous, trace limestone, trace sand, scattered yellow green fluorescence, yellow green streaming cut with bright halo.

Well B: Chruszch 43X-29F, XTO Energy Inc

10880 – 10910ft Shale (70%): very light to medium gray, soft to firm, blocky to subplaty, waxy to earthy, trace silt, slightly dolomitic. Siltstone (20%): white to light brown, firm to hard, platy to subblocky, occasionally slightly argillaceous, trace sandy, trace slightly dolomitic, tight, dull yellow fluorescence, poor to fair yellow milky cut. Shale (10%): black, firm, blocky, subvitreous, carbonaceous, trace pyrite, noncalcareous, no fluorescence, fair yellow milky cut.

Well C: Pumpkin 148-93-14C-3H TF, Enerplus Resources Corp

10248 – 10251ft Shale: Black, sub blocky-platy, carbonaceous, disseminated pyrite, non-calcareous, no visible shows.

10307 – 10310ft Shale: Dark grey brown, blocky to sub-blocky, firm slightly dolomitic, no visible fluorescence or cut.

Appendix B

Measured Shale Properties from Nanoindentation Tests

Sample Number	Average Young's Modulus (GPa)	Hardness (GPa)	Sample Source	Primary Mineral Composition
#1(Indentations parallel to the bedding)	50	3.0	Middle Bakken Well: LINSETH 13-12HW Depth: 11135.4ft	Quartz (48.10%), Muscovite (35.90%), Anorthoclase (5.7%)
#1(Indentations perpendicular to the bedding)	45	3.0	Middle Bakken Well: LINSETH 13-12HW Depth: 11135.4ft	
#2	78	5.1	Middle Bakken Well: Chruszch 43-29F Depth: 10888.35ft	Illite (46.60%), Quartz (14.90%), Dolomite (14.20%)
#3	75	4.8	Lower Bakken Well: Chruszch 43-29F Depth: 10932.95ft	
#4	38	3.2	Lower Bakken Well: Pumpkin 148-93- 14C-13H TF Depth: 10249.00ft	
#5	51	2.4	Lower Bakken Well: Pumpkin 148-93-14C-13H TF Depth: 10309.00ft	

Appendix C

Preprocessing

```
/FILNAM          ! SPECIFY JOBNAME

/PREP7           ! ENTER PREPROCESSOR

ET, 1, 183       ! ELEMENT TYPE 1 IS PLANE 183

KEYOPT, 1, 3, 1  !

MP, EX, 1, 1141000 ! DIAMOND INDENTER MAT PROPS

MP, NUXY, 1, 0.07 !

MP, EX, 2, 52794 ! ROCK MAT PROPS

MP, NUXY, 2, 0.23 !

TB, BISO, 2, 1   ! BILINEAR ISOTROPIC HARDENING RULE

TBTEMP, 0        !

TBDATA, 1, 550, 0 ! ROCK YIELD STRENGTH

K, 1              ! CREAT KEYPOINTS

K, 2, 3

K, 3, 8

K, 4, 0, 3.5

K, 5, 3, 3.5

K, 6, 8, 3.5

K, 7, 0, 5

K, 8, 3, 5

K, 9, 8, 5

K, 10, 0, 6
```

K, 11, 3, 6

K, 12, 8, 6

L, 1, 2

! CREATE LINES

L, 2, 3

L, 4, 5

L, 5, 6

L, 7, 8

L, 8, 9

L, 10, 11

L, 11, 12

L, 1, 4

L, 2, 5

L, 3, 6

L, 4, 7

L, 5, 8

L, 6, 9

L, 7, 10

L, 8, 11

L, 9, 12

AL, 1, 3, 9, 10

! CREATE AREAS

AL, 2, 4, 10, 11

AL, 3, 5, 12, 13

AL, 4, 6, 13, 14

AL, 5, 7, 15, 16

AL, 6, 8, 16, 17

H=0.05

K, 23, 0, 6+H

K, 24, 2.475, 7+H

K, 25, 2.475, 8+H

K, 26, 0, 8+H

L, 23, 24

L, 24, 25

L, 25, 26

L, 26, 23

AL, 18, 19, 20, 21

LESIZE, 7, , , 40

! SPECIFY LINE DIVISIONS

LESIZE, 5, , , 40

LESIZE, 3, , , 40

LESIZE, 1, , , 40

LESIZE, 8, , , 30, 4

LESIZE, 6, , , 30, 4

LESIZE, 4, , , 30, 4

LESIZE, 2, , , 30, 4

LESIZE, 9, , , 20, 1/4

LESIZE, 10, , , 20, 1/4

LESIZE, 11, , , 20, 1/4

LESIZE, 12, , , 20

LESIZE, 13, , , 20

LESIZE, 14, , , 20

LESIZE, 15, , , 20

LESIZE, 16, , , 20

LESIZE, 17, , , 20

LESIZE, 18, , , 30

LESIZE, 19, , , 30

LESIZE, 20, , , 30

LESIZE, 21, , , 30

GPLOT

TYPE, 1 ! SWITCH TO ET 1

MSHKEY, 1 ! ENFORCE MAPPED MESHING

MAT, 2 ! SWITCH TO MATERIAL 2

AMESH, 1, 2 ! CREATE MESH

MAT, 2 ! SWITCH TO MATERIAL 2

AMESH, 3, 4 ! CREATE MESH

MSHKEY, 0 ! ENFORCE MAPPED MESHING

AMESH, 5 ! CREATE MESH

MSHKEY, 1 ! ENFORCE MAPPED MESHING

AMESH, 6 ! CREATE MESH

MAT, 1 ! SWITCH TO MATERIAL 1

AMESH, 7 ! CREATE MESH

```
GPLOT          ! CONTROL GENERAL PLOTTING
NSEL, S, LOC, Y, 6    ! SELECT NODES AT Y= 6
CM, CONTACT123, NODE
ALLSEL
LSEL, S, P
NSLL, S, 1
CM, TARGET123, NODE
ALLSEL
```


Solution (Xeed, 2015)

```
/SOLU                ! ENTER SOLUTION PROCESSOR
SOLCONTROL, ON      ! TURN OFF SOLUTION CONTROLS
ANTYPE, STATIC      ! SPECIFY ANALYSIS TYPE AS STATIC
NSEL, S, LOC, Y, 8.05  ! SELECT NODES AT Y=8.05
D, ALL, UY          ! CONSTRAIN Y-DISP AT SELECTED NODE
ALLSEL              ! SELECT EVERYTHING
NSEL, S, LOC, X, 0    ! SELECT NODE AT X=0
D, ALL, UX          ! CONSTRAIN X-DISP AT SELECTED NODE
ALLSEL              ! SELECT EVERYTHING
*DIM, DIS, ARRAY, 57  ! INITIALIZE ARRAY PARAMETER DIS
A=0                 ! INITIALIZE PARAMETER A
*DO, I, 1, 36        ! START DO LOOP FOR LOADING
DIS (I) = A         ! STORE DISP VALUE IN DIS FOR CURRENT LS
A=A+.01035          ! UPDATE PARAMETER A
*ENDDO              ! END DO LOOP ON LOADING
B=0.005             ! INITIALIZE PARAMETER B
*DO, I, 37, 57      ! START DO LOOP FOR UNLOADING
DIS (I) =A-B        ! STORE DISP VALUE IN DIS FOR CURRENT LS
B=B+.005            ! UPDATE PARAMETER B
*ENDDO              ! END DO LOOP ON UNLOADING
NLGEOM, ON          ! TURN ON NONLINEAR GEOMETRY EFFECTS
AUTOTS, ON          ! TURN ON AUTOMATIC TIME STEPPING
```

```

OUTRES, ALL, ALL      ! CONTROL SOLUTION DATA WRITEN TO
                      ! DATABASE

OUTPR, ALL, ALL      ! CONTROL SOLUTION PRINTOUT

NROPT, FULL, , OFF   ! USE FULL NEWTON-RAPHSON WITH
                      ! NO APAPTIVE DESCENT

NEQIT, 100           ! USE MAXIMUM 100 EQUILIBRIUM
                      ! ITERATIONS

ALLSEL               ! SELECT EVERYTHING

*DO, I, 1, 57        ! START DO LOOP FOR WRITING LOAD STEPS

NSEL, S, LOC, Y      ! SELECT NODES AT Y=0

D, ALL, UX           ! CONSTRAIN X-DISP AT SELECTED NODES

D, ALL, UY, DIS (I)  ! SPECIFY Y-DISP ALONG THE BOTTOM
                      ! SURFACE OF THE ROCK

ALLSEL               ! SELECT EVERYTHING

LSWRITE, I           ! WRITE LOAD STEP FILE

*ENDDO               ! END DO LOOP ON WRITING LOAD STEPS

LSSOLVE, 1, 57       ! SOLVE FROM LS FILES (1 TO 57)

```

Postprocessing (Erdogan, 2005)

```
/POST1                ! ENTER GENERAL POSTPROCESSOR

*DO, J, 1, 57         ! LOOP OVER LOAD STEPS

SET, J                ! READ RESULTS SET

NSEL, S, LOC, Y       ! SELECT NODES AT Y=0

*GET, NUMNOD, NODE, 0, COUNT  ! STORE # OF NODES IN NUMNOD

*GET, CURNOD, NODE, 0, NUM, MIN  ! STORE MIN NODE # TO
                                ! CURNOD

SUM= 0                ! INITIALIZE TOTAL REACTION FORCE

*DO, I, 1, NUMNOD     ! LOOP OVER SELECTED NODES

*GET, RFY, NODE, CURNOD, RF, FY  ! STORE Y REACT. FORCE IN
                                ! RFY

SUM=SUM+RFY           ! UPDATE TOTAL REACTION FORCE

CURNOD= NDNEXT (CURNOD)  ! UPDATE CURRENT NODE
                                ! NUMBER

*ENDDO                ! END LOOP OVER SELECTED NODES

DISJ= DIS (J)         ! STORE CURRENT INDENTATION
                                ! DEPTH TO PARAMETER DISJ

/OUTPUT, NANO, OUT, , APPEND  ! REDIRECT OUTPUT TO FILE

*VWRITE, DISJ, SUM     ! WRITE DISJ AND SUM TO FILE
(E16.8, 5X, E16.8)    ! FORMAT STATEMENT

/OUTPUT                ! REDIRECT OUTPUT TO FILE

*ENDDO                ! END LOOP OVER LOAD STEPS
```

NOMENCLATURE

A:	the contact area between nanoindenter and sample
d:	distance
E:	Young's modulus of the sample
E_i :	Young's modulus of Berkovich indenter tip
E_r :	reduced Young's modulus of Berkovich indenter tip
h:	displacement depth
h_f :	the final depth
h_{max} :	maximum displacement depth
P:	load
P_{max} :	peak load
S:	the slope of unloading curve
ν :	Poisson's ratio of the sample
ν_i :	Poisson's ratio of Berkovich indenter tip
θ :	angle
λ :	wavelength

REFERENCES

- Almeida, C.M., R. Prioli, and F.A. Ponce. 2008. Effect of Native Oxide Mechanical Deformation on InP nanoindentation. *J. Appl. Phys.* 104, 113509:1–113509:6.
- Anderson, H.W. and J.S. Dodd. 1966. Finite Element Method Applied to Rock Mechanics. In Proceedings of the 1st ISRM Congress, Lisbon, Portugal, 25 September-1 October.
- Anna, L.O., R. Pollastro, and S.B. Gaswirth. 2013. Williston Basin Province—Stratigraphic and Structural Framework to a Geologic Assessment of Undiscovered Oil and Gas Resources, Chap. 2 of U.S. Geological Survey.
- Ban, H., P. Karki, and Y.R. Kim. 2014. Nanoindentation Test Integrated with Numerical Simulation to Characterize Mechanical Properties of Rock Materials. *Journal of Testing and Evaluation*, Vol. 42, No. 3, pp 1-10.
- Bhowmik, R., K. S. Katti, and D. R. Katti. 2007. Mechanics of Molecular Collagen is Influenced by Hydroxyapatite in Natural Bone. *Journal of Materials Science*, Vol. 42, pp. 8795-8803.
- Cherian, B.V., E.S Stacey, R. Lewis, F.O. Iwere, R.N. Heim, and S.M. Higgins. 2012. Evaluating Horizontal Well Completion Effectiveness in a Field Development Program, Paper SPE 152177 in Proceedings of the Hydraulic Fracturing Technology Conference, 6-8 February, the Woodlands, Texas.
- Chi, C. 2009. 2-D Finite Element Modeling for Nanoindentation and Fracture Stress Analysis. M.Sc. Thesis, University of South Florida, Florida, USA.
- Ch, S.R., and C.E. Reddy. 2008. Finite Element Modeling of Nanoindentation to Extract Load-Displacement Characteristics of Bulk Materials and Thin Films. *Indian*

Journal of Pure & Applied Physics, Vol.47, January 2009, pp. 54-59.

David, J. S., L.M. Costa and M.S. Andrade. 2006. Calculating the Elastic Modulus from Nanoindentation and Microindentation Reload Curves. *Materials Characterization* 58 (2007) 380-389.

Dejun, M., C. Ong, J. Liu and J. He. 2003. Determination of Young's Modulus by Nanoindentation. *Science in China Ser. E Engineering & Materials Science* (2004), Vol. 47, No.4, 398-408.

Erdogan, M. and I. Guven. 2005. *The Finite Element Method and Applications in Engineering Using Ansys*. Springer Science & Business Media, LLC, New York.

Fengyuan, C. and R. Chang. 2005. Numerical Simulation of Nanoindentation by Finite Element Method. In *Proceedings of the 29th National Conference on Theoretical and Applied Mechanics*, Hsinchu, Taiwan, R.O.C., December 16-17.

Fengyuan, C. and R. Chang. 2007. Study of the Effect of Imperfect Tips on Nanoindentation by FEM. *Journal of Mechanical Science and Technology* 21, 1471~1476.

Ghosh, P., D. R. Katti, and K. S. Katti. 2007. Mineral Proximity Influences Mechanical Response of Proteins in Biological Mineral-Protein Hybrid Systems. *Biomacromolecules*, Vol. 8, pp. 851-856.

Hay, J.L., and G.M. Pharr. 2000. Instrumented Indentation Testing. *ASM Handbook*, 232-243.

Hester, T.C., and Schmoker, J.W. 1985. Selected Physical Properties of the Bakken Formation, North Dakota and Montana Part of the Williston Basin: U.S. Geological Survey Oil and Gas Investigations Chart, OC-126, 1 sheet.

- Jun, H. 2015. Study about Petrophysical and Geomechanical Properties of Bakken Formation. Ph.D. Dissertation, University of North Dakota, U.S.
- Katti, D.R., K.S. Katti, and K. Alstadt. 2013. An Insight into Molecular Scale Interactions and In-Situ Nanomechanical Properties of Kerogen in Green River Oil Shale. *Poromechanics V*, Vol. 1, pp. 2510-2516.
- Kouqi, L. 2017. Fracture Toughness Measurement of Shales Using Nano-indentation: The Bakken case study. In *Proceedings of the 51st US Rock Mechanics/ Geomechanics Symposium*, San Francisco, CA, USA, 25-28 June.
- Ma, S.M., A.S. Al-Muthana and R.N. Dennis. 2002. Use of Core Data in Log Lithology Calibration: Arab-D Reservoir, Abqaiq and Ghawar Fields. In *Proceedings of the SPE Annual Technical Conference and Exhibition*, San Antonio, Texas, USA, 29 September-2 October.
- Meissner, F.F. 1978. Petroleum Geology of the Bakken Formation, Williston Basin, North Dakota and Montana, in D. Rehg., (ed.), *The Economic Geology of the Williston Basin: Proceedings of the Montana Geological Society, 24th Annual Conference*, pp. 207-227.
- Ming, L. 2016. An Examination of the Mineralogy and Lithology of the Bakken Shale with Implications upon the Bakken Petroleum System, Southeastern Saskatchewan. M.Sc. Thesis, University of Regina, Saskatchewan, Canada.
- Nojabaei, B., R.T. Johns and L. Chu. 2013. Effect of Capillary Pressure on Phase Behavior in Tight Rocks and Shales, *SPE Reservoir Evaluation & Engineering Journal*, July 2013.
- Oliver, W. C. and G. M. Pharr, 1992. Improved Technique for Determining Hardness

- and Elastic Modulus Using Load and Displacement Sensing Indentation Experiments, *Journal of Materials Research*, Vol. 7, pp. 1564-1583.
- Oliver, W.C. and G.M. Pharr, 2003. Measurement of Hardness and Elastic Modulus by Instrumented Indentation: Advances in Understanding and Refinements to Methodology. *Journal of Materials Research*, Vol. 19, No. 1, Jan 2004.
- Pang, M., D.F. Bahr and K.G. Lynn. 2003. Effects of Zn Addition and Thermal Annealing on Yield Phenomena of CdTe and Cd_{0.96}Zn_{0.04}Te Single Crystals by Nanoindentation. *Appl. Phys. Lett.*, 82, 1200-1202.
- Price, L.C. 2000. Origin and Characteristics of the Basin-Centered Continuous-Reservoir Unconventional Oil-resource Base of Bakken Source System, Williston Basin. Energy and Environmental Research Center.
- Shengrui, J., C. Guoju and H. Weimin. 2013. Mechanical Properties of Cu₂O Thin Films by Nanoindentation. *Journal of Materials*, Vol. 6, pp. 4505-4513
- Shukla, P., V. Kumar, M. Curtis, C.H. Sondergeld and C.S. Rai. 2013. Nanoindentation Studies on Shales. In Proceedings of the 47th US Rock Mechanics/Geomechanics Symposium, San Francisco, CA, USA, 23-26 June.
- Tran, T., P. Sinurat, and R.A. Wattenbarger. 2011. Production Characteristics of the Bakken Shale Oil, Paper SPE 145684 in Proceedings of the SPE Annual Technical Conference and Exhibition, Denver, Colorado, 30 October-2 November.
- Wang, C, and Z. Zeng. 2011. Overview of Geomechanical Properties of Bakken Formation in Williston Basin, North Dakota. In Proceedings of the 45th US Rock Mechanics/ Geomechanics Symposium, San Francisco, CA, June 26–29,

201.

Weinbrandt, R.M. and I. Fatt. 1969. Scanning Electron Microscope Study of the Pore Structure of Sandstone. In Proceedings of the 11th U.S. Symposium on Rock Mechanics (USRMS), , Berkeley, CA, 16-19 June.

Wenfeng, L., A. Sakhaee-Pour. 2016. Macroscale Young's Moduli of Shale Based on Nanoindentations, *Petrophysics*, vol. 57, No.6, Page 597-603.

Xeed, G. 2015. Nano-Indentation Using ANSYS on Mechanical APDL Coding 1. Retrieved from <http://youtu.be/5FmRd00fG3w>.